# Angular distribution of characteristic photons after radiative electron capture at strong central fields

E. G. Drukarev,[1,2] X. Ma,[2,3] A. I. Mikhailov,[1] I. A. Mikhailov,[1] and P. H. Mokler[2,4]
[1]*Petersburg Nuclear Physics Institute, Gatchina, St. Petersburg 188300, Russia*
[2]*GSI, 64291 Darmstadt, Germany*
[3]*Institute of Modern Physics, Lanzhou, 730000, China*
[4]*Institut für Atom-und Molekülphysik, Justus-Liebig University, 35392 Giessen, Germany*
(Received 26 May 2006; published 17 August 2006)

We investigate the difference in the angular distribution of Ly-$\alpha_1$ and $K\alpha_1$ photons from hydrogenlike and heliumlike ions of uranium after radiative electron capture to the $L$ shell. The strong anisotropy in the former case is changed to a very small one in the latter case. Our calculations support the observation. The effect takes place even in the limiting case of noninteracting electrons, being caused by the Pauli principle.

DOI: 10.1103/PhysRevA.74.022717 PACS number(s): 32.80.−t, 32.80.Wr

## I. INTRODUCTION

In connection with radiative electron capture (REC) to excited states of heavy ions a radiative transition to the ground state will also occur. Experiments on the angular distribution of those cascade photons in collisions of uranium ions with light target atoms provided different results for initially bare uranium nuclei $U^{92+}$, and for one-electron uranium ions $U^{91+}$ in the ground state. While exhibiting a strong angular dependence for the distribution of Ly-$\alpha_1$ photons in the former case [1], the experiment provided a nearly isotropic distribution for the corresponding $K\alpha_1$ photons in the latter case [2]. In both cases the active electron is a $2p_{3/2}$ one. Both experiments were performed at the gas-jet target of the heavy ion storage ring ESR at GSI in Darmstadt. In this paper we present in Sec. II the details of the experimental findings, in Secs. III and IV as well as in the Appendixes, we present the theoretical description. The results of the calculations are in good agreement with the experimental findings.

In the rest frame of the uranium nucleus the process can be viewed as a two-photon capture of a continuum electron to the $1s$ state of the uranium nuclei (or of the single-electron ion $U^{91+}$) with an $L$-shell intermediate state. Thus the process proceeds as radiative electron capture to the $L$ shell, followed by a radiative transition to the $K$ shell. In the case of bare $U^{92+}$ these are the chains

$$i \to 2p_{3/2} \to 1s_{1/2};$$

$$i \to 2p_{1/2} \to 1s_{1/2}; \quad i \to 2s_{1/2} \to 1s_{1/2}, \tag{1}$$

with "$i$" denoting the incoming continuum electron. In the case of the hydrogenlike ions $U^{91+}$ the chains are

$$i + 1s_{1/2} \to 2\ ^1P_1 \to 1\ ^1S_0; \; i + 1s_{1/2} \to 2\ ^3P_2 \to 1\ ^1S_0;$$

$$i + 1s_{1/2} \to 2\ ^3P_1 \to 1^1S_0; \quad i + 1s_{1/2} \to 2\ ^3S_1 \to 1\ ^1S_0;$$

$$i + 1s_{1/2} \to 2\ ^3P_0 \to 1\ ^1S_0; \tag{2}$$

$$i + 1s_{1/2} \to 2\ ^1S_0 \to 1\ ^1S_0.$$

The REC two-photon process is displayed schematically in Fig. 1 for both cases. In the experiments only two x-ray lines can be separated: for initially bare $U^{92+}$ the Ly-$\alpha_1$ and Ly-$\alpha_2$ lines where the second one comprises also the photons from the $M1$ transition $2s_{1/2} \to 1s_{1/2}$ [compare the first and second lines in Eq. (1), respectively]; for the initially one-electron system $U^{91+}$ each line comprises two transitions—for $K\alpha_1$ the $2\ ^1P_1$ and the $2\ ^3P_2 \to 1\ ^1S_0$ transitions and for $K\alpha_2$ the $2\ ^3P_1$ and $2\ ^3S_1$ transitions to the ground state [cf. the first and second lines in Eq. (2), respectively]. In both cases the observed lines correspond separately to transitions involving active electrons with the total angular momentum either $j=3/2$ or $j=1/2$. Levels including an intermediate $2p_{3/2}$ electron are the levels of concern contributing mainly to an anisotropic photon emission (Ly-$\alpha_1$ and $K\alpha_1$, respectively).

In the single-electron case the $2p_{3/2}$ state decays to $1s_{1/2}$ mainly by an $E1$ transition, with a small correction coming from the $M2$ mode. In the two-electron case the system of $2p_{3/2}$ and $1s_{1/2}$ electrons forms $2P_J$ states with $J=1,2$, which provides the $K\alpha_1$ line. While the system of $2p_{1/2}$ and $1s_{1/2}$ electrons forms $2P_J$ states with $J=0,1$, providing the $K\alpha_2$ line in the case $J=1$. A single-photon transition $2\ ^3P_0 \to 1\ ^1S_0$ is forbidden by the selection rules and the two-photon decay is the main mode, which does not contribute to the $K\alpha_2$ line. Additionally the $2\ ^3S_1$ decay of the $2s_{1/2}$ and $1s_{1/2}$ system contributes to the $K\alpha_2$ line and cannot be distinguished experimentally from the $2\ ^3P_1$ transition to the ground state (and has to be considered in the calculations separately). The states $2\ ^1P_1$ and $2\ ^3P_2$ decay by the emission of $E1$ and $M2$ photons, respectively. They are not distinguished in the experiment but should be treated separately in the calculations. The $E1$ transition $2\ ^1P_1 \to 1\ ^1S_0$ provides the main channel for the decay of the state $2\ ^1P_1$ while the other channels can be neglected. In the case of the decay of the state $2\ ^3P_2$ the $M2$ transition $2\ ^3P_2 \to 1\ ^1S_0$ gives only about 70% of the total width with the two-photon chain $2\ ^3P_2 \to 2\ ^3S_1 \to 1\ ^1S_0$ adding the rest. The latter channel is not detected within the $K\alpha_1$ in the experiment, being transferred to the $K\alpha_2$ line. Note that we are using the conventional notation $2\ ^3P_1$ and $2\ ^1P_1$ for the two-electron states with $J=1$ formed by $1s_{1/2}, 2p_{1/2}$ and $1s_{1/2}, 2p_{3/2}$ electrons, although this nonrelativistic notation is somewhat misleading: the upper indices in the notations $2\ ^3P_1$ and $2\ ^3P_1$ do not have meaning of the total spin.

 ©2006 The American Physical Society

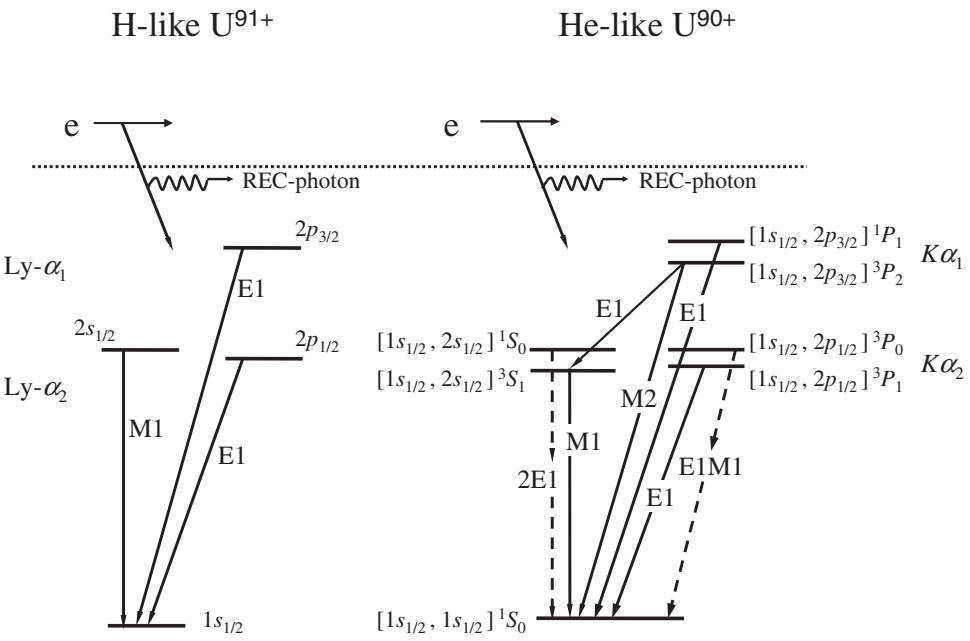


FIG. 1. The L-REC two-photon process for initially bare and hydrogenlike U ions [left and right side, respectively, cf. Eqs. (1) and (2)].

The experiments discussed in Sec. II show isotropic emission for the decay of intermediate $s_{1/2}$ and $p_{1/2}$ electrons both for the bare and hydrogenlike cases. For intermediate $p_{3/2}$ states a strong anisotropy is observed for initially bare ions [1], whereas a practically isotropic emission pattern was found for the initially hydrogenlike case [2].

We shall refer to the photons, emitted in the first and second steps of the chains (1) and (2), as the "first" and "second" photons. In the theoretical part of the paper we calculate the angular distribution of the second photon $\frac{d\sigma}{d\Omega_2}$ (in the reference frame of the ion) with the solid angle $\Omega_2(t_2,\varphi_2)$, while $t_2=\frac{(\boldsymbol{p}\cdot\boldsymbol{k}_2)}{pk_2}=\cos\theta_{\mathrm{c.m.}}$, where $\theta_{\mathrm{c.m.}}$ and $\varphi_2$ are the polar and azimuthal angles of the photon momentum $\boldsymbol{k}_2$; $\boldsymbol{p}$ and $\boldsymbol{k}_2$ denote the three-dimensional momenta of the initial state electron and of the second photon. We present

$$\frac{d\sigma}{d\Omega_2}=\frac{1}{4\pi}\sigma F(t_2,\varphi_2). \tag{3}$$

After integration over the azimuthal angle we find

$$\frac{d\sigma}{dt_2}=\frac{1}{2}\sigma f(t_2). \tag{4}$$

If the function $F$ does not depend on $\varphi_2$, we find $F(t_2)=f(t_2)$. For the isotropic distribution we have $f(t_2)=1$.

The deviations of the function $f(t_2)$ from unity indicate that the second photon "remembers" the direction of the incoming electron. For the dipole transitions the angular distribution can be written as

$$f(t_2)=1+\beta_2 P_2(t_2), \tag{5}$$

with $P_2(t_2)$ being the second-order Legendre polynomial, while $\beta_2$ is the anisotropy parameter.

The amplitude of the process can be presented as

$$F=\sum_x F_x;\quad F_x=\frac{A_x B_x}{\varepsilon_f+\omega_2-(\varepsilon_x-i\Gamma_x/2)}, \tag{6}$$

with $x$ labeling the quantum numbers (angular momentum and parity) of the intermediate states on the $L$ shell with the binding energies $\varepsilon_x$ and the total width of the single-particle state $\Gamma_x$; $\varepsilon_f$ and $\omega_2$ denote the energies of the final state and of the second photon. The amplitudes

$$A_x=\langle\Psi_f|\gamma^{(2)}|\Psi_x\rangle;\quad B_x=\langle\Psi_x|\gamma^{(1)}|\Psi_i\rangle, \tag{7}$$

describe the radiation of the second and first photon, while "$i$" and "$f$" denote the initial and final states of the electrons. The operators $\gamma^{(i)}$ describe the interactions of the first and second photon with the electrons.

In the case of capture by a bare nucleus, the final and initial electronic states are just the single-particle $1s_{1/2}$ state and the continuum state in the Coulomb field of the nucleus. The intermediate states in the $L$ shell can be $2s_{1/2}$, $2p_{1/2}$, and $2p_{3/2}$. For capture by a bare nucleus Eq. (6) can be presented as

$$F=F_{2s_{1/2}}+F_{2p_{1/2}}+F_{2p_{3/2}};\quad F_x=\sum_m \frac{A_{xm}B_{xm}}{\varepsilon_f+\omega_2-(\varepsilon_x-i\Gamma_x/2)}; \tag{8}$$

here $m$ denotes the projection of the total angular momentum $j$.

For the capture by a single-electron ion in the ground state the final state is $1\,{}^1S_0$. The intermediate states are $2P_J$ with $J=0,1,2$ ($2\,{}^3P_0, 2\,{}^3P_1, 2\,{}^1P_1, 2\,{}^3P_2$) and $2S_J$ with $J=0,1$ ($2\,{}^1S_0$ and $2\,{}^3S_1$). The states $2\,{}^1S_0$ and $2\,{}^3P_0$ cannot decay by radiation of a single photon and thus do not contribute directly to the line emission of interest. In this case Eq. (6) takes the form

$$F = \sum_x F_x; \quad F_x = \sum_M \frac{A_{xM} B_{xM}}{\varepsilon_f + \omega_2 - (\varepsilon_x - i\Gamma_x/2)},$$

with $M$ being the projection of the total angular momentum $J$ of the two-electron system.

The amplitudes $F_{j(J)}$ (this means $F_j$ or $F_J$) determine the distributions $\frac{d\sigma_{j(J)}}{d\Omega_1 d\Omega_2}$ with $\Omega_{1,2}$ being the solid angles of the emitted photons. Summation over the photon polarizations and averaging over the spin states of the initial electron(s) should be carried out. Besides the angular distribution functions $f(t_2)$ determined by Eq. (4) we introduce the partial distribution functions determined as

$$\frac{d\sigma_{j(J)}}{dt_2} = \frac{1}{2}\sigma_{j(J)} f_{j(J)}(t_2). \tag{9}$$

The anisotropy of the radiation of the second photon is due to the dependence of the weights $B^2_{xm}(B^2_{xM})$, integrated over the solid angle of the first photon, on the value of $m(M)$. Otherwise the emission of the two photons goes on independently and the distribution $d\sigma/dt_2$ is isotropic.

Besides the angular distribution in the rest frame of the heavy projectile, which actually coincides with the center of mass (c.m.) frame, it is instructive to provide the results in the rest frame of the light target, which coincides with the laboratory system. Since the experiments detect the angular distribution of the intensity ratio of the $\alpha_1$ to $\alpha_2$ lines, we must transform the ratios

$$R(t_2) = \frac{f_{\alpha_1}(t_2)}{f_{\alpha_2}(t_2)} \tag{10}$$

to the laboratory system. Thus we must find

$$R(\tau_2) = \frac{f_{\alpha_1}(t_2(\tau_2))}{f_{\alpha_2}(t_2(\tau_2))}, \tag{11}$$

with $\tau_2 = \frac{(\boldsymbol{p}\cdot\boldsymbol{k}_2)}{pk_2}$ in the laboratory system [3]. One can write

$$t_2(\tau_2) = \frac{\tau_2 - \beta}{1 - \tau_2\beta} \tag{12}$$

with $\beta$ being the electron velocity (in units of the velocity of light) in the rest system of the nucleus of uranium—see, e.g., [3].

For the dipole transitions one can write [see also Eq. (5)]

$$f(t_2) = a - bt_2^2, \tag{13}$$

while $a$ and $b$ do not depend on $t_2$. In this case the anisotropy can be described by the shape parameter

$$\mu = \frac{f(t_2 = 0)}{f(t_2 = 1)} = \frac{f(\tau_2 = \beta)}{f(\tau_2 = 1)}. \tag{14}$$

For $b > 0$ we can write

$$\mu = \frac{f_{\max}}{f_{\min}}, \tag{15}$$

while for $b < 0$ we have $\mu = \frac{f_{\min}}{f_{\max}}$. For transitions of the higher multipolarity Eq. (15) can be viewed as a definition of the anisotropy characteristics $\mu$. However, Eq. (14) may be not true since higher powers of $t_2$ are present in the expression for the function $f(t_2)$. As we shall show below, in the particular case of the $M2$ transition $2\,^3P_2 \to 1\,^1S_0$ the terms proportional to $t_2^4$ cancel in the angular distribution. Thus the function $f(t_2)$ has the form (13) and the value of the parameter $\mu$ defined by Eq. (15) is the same in both systems of reference. Also, due to the cancellation of the terms $t_2^4$ in this particular $M2$ transition, all the angular distributions considered in the paper can be expressed by Eq. (5) with the anisotropy parameter, expressed in terms of $\mu$ being (for $b > 0$)

$$\beta_2 = \frac{1 - \mu}{\frac{1}{2} + \mu}. \tag{16}$$

In the case of a capture to an electronic shell of a bare nucleus the electrons can be described by relativistic Coulomb functions. In the case of the single-electron ion $U^{91+}$ we describe the two-electron states by antisymmetric compositions of products of relativistic Coulomb functions. Inclusion of the electron interactions would provide corrections of the order $Z^{-1}$ with $Z$ standing for the nuclear charge. This is about 1% in the case of uranium. Thus the influence of the second electron ("spectator") manifests itself mainly via the Pauli principle.

Another approximation is prompted by the specific conditions of the experiment. The lowest characteristic energies of the projectile are $E \approx 100$ MeV/u. This corresponds to electron energies in the c.m. frame close to $\varepsilon = 50$ keV. Hence in this case the value of its three-dimensional momentum is $p = 232$ keV/$c$ (the nonrelativistic value is $p = 226$ keV/$c$), while the momentum of the first photon is $k_1 = 80$ keV/$c$. Thus $k_1^2/p^2 = 0.12$ can be treated as a small parameter. We shall carry out the calculations in the lowest order of expansion in powers of $k_1^2/p^2$. This approximation provides better accuracy for the shape of the angular distribution than for the absolute values of the cross sections due to the common factors with stronger dependence on $k_1^2$. In this approach the radiation of the first photon is an $E1$ transition. At larger energies of the projectiles the corrections of the order $\frac{(m\alpha Z)^2}{p^2}$ become smaller, while a relativistic treatment of the incoming electron becomes increasingly important.

This approach enabled us to obtain analytical expressions for the anisotropy effects in the Ly-$\alpha_1$ series and to trace their energy dependence. The reasonable results encouraged us to apply the approach to investigate the anisotropy in the $K\alpha_1$ radiation. We show that the large difference in the asymmetry effects for these two cases is caused by the Pauli principle.

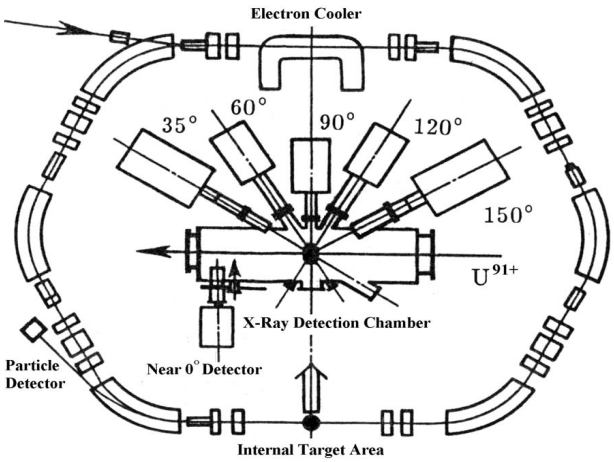


FIG. 2. Experimental arrangement at the heavy ion storage ring ESR at GSI Darmstadt. The central insert gives the target chamber at the gas-jet target together with the different x-ray detectors.

## II. MEASUREMENTS ON THE ANGULAR DISTRIBUTION OF REC PHOTONS IN TWO-PHOTON PROCESS

### A. Experimental arrangement

Radiative electron capture to heavy bare and heavy few-electron ions has been extensively studied at the heavy ion storage ring ESR over the past years [1,4–14]. Typically 50–300 MeV/u heavy ions ($79<Z<93$) colliding with light targets ($N_2$ and $H_2$) were investigated showing good agreement between advanced theory (see, e.g., [15]) and experiments for the direct REC process. During these experiments a bunch of solid state x-ray detectors monitored the angular distribution of the emitted x rays in coincidence with the heavy ions having captured one electron. The typical experimental arrangement at the gas-jet target of the ESR is shown in Fig. 2; for details see, e.g., [1,16]. For capture into higher shells like the $L$ shell of a heavy atom, in addition to the REC radiation the cascading photons to the ground state were observed as well [6,9,12,13]. Here intensity ratios like Ly-$\alpha_1$/Ly-$\alpha_2$ (initially bare ion case) and $K\alpha_1/K\alpha_2$ (initially hydrogenlike case) could be determined with high accuracy.

Due to normalization uncertainties the angular distributions for the intensities of the single lines provide larger inaccuracies—quite larger than those for the intensity ratios $\frac{\alpha_1}{\alpha_2}$. Moreover, for the intensity ratios the solid angle transformation from the emitter frame of the moving ion (c.m. system) to the observation frame in the laboratory system (laboratory system) cancels; only the angles themselves have to be transformed. Hence we discuss in the following the angular dependence of the intensity ratios for the two corresponding cases:

(1) Ly-$\alpha_1$/Ly-$\alpha_2$ intensity ratio for the REC two-photon process in 309.7 MeV/u $U^{92+}$-$N_2$ collisions [1], and

(2) $K\alpha_1/K\alpha_2$ intensity ratio for the REC two-photon process in 102 MeV/u $U^{91+}$-$H_2$ collisions [2].

The energy resolution of the solid state detectors is not good enough to separate closely spaced transitions; in both cases each of the two corresponding lines Ly-$\alpha_{1,2}$ and $K\alpha_{1,2}$ could be resolved and mostly two transitions contribute to the lines, cf., Fig. 1. However, the lines can be clearly separated into contributions from $j=1/2$ and $j=3/2$ electrons in the $L$ shell giving good access to the role of the (total) angular momentum in the intermediate states.

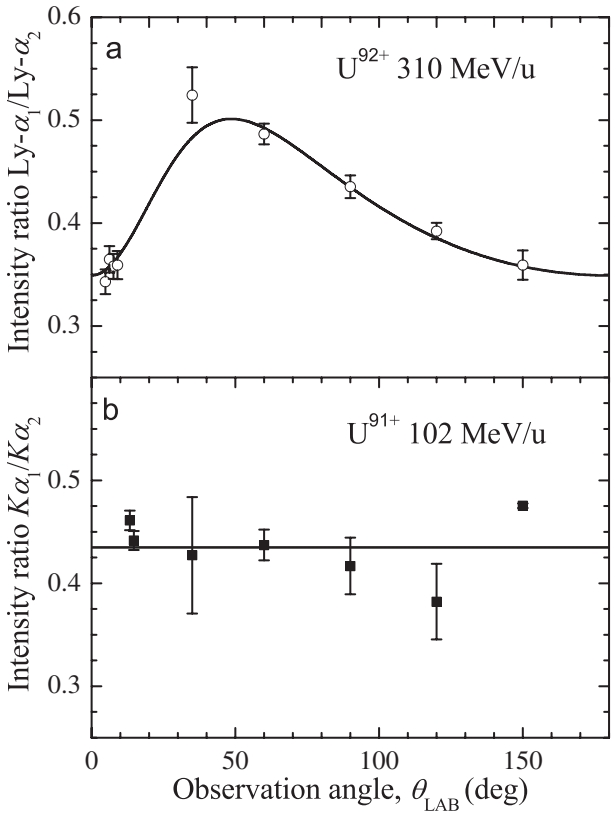


FIG. 3. Angular distribution of the $\alpha_1/\alpha_2$ intensity ratios in the laboratory frame for (a-top): Ly-$\alpha$ at 310 MeV/u $U^{92+}\rightarrow N_2$ collisions (initially bare ion case) [1] and for (b-bottom): $K\alpha$ at 102 MeV/u $U^{91+}\rightarrow H_2$ collisions (initially H-like ion case) [2]. The curves give the best fits to the experimental data.

### B. Ly-$\alpha_1$/Ly-$\alpha_2$ intensity ratio for REC in $U^{92+}$

As discussed in detail in Ref. [1] the Ly-$\alpha_2$ line originating from $j=1/2$ $L$ electrons shows an isotropic emission pattern. Hence we can use the angular dependence of the intensity ratio Ly-$\alpha_1$/Ly-$\alpha_2$ as only caused by the anisotropy of the Ly-$\alpha_1$ emission originating from the intermediate $j=3/2$ state. The angular dependence of the Ly-$\alpha_1$/Ly-$\alpha_2$ ratio is shown in Fig. 3(a), exhibiting a pronounced anisotropic distribution. We give here—for 310 MeV/u initially bare $U^{92+}$ ions—the intensity ratio Ly-$\alpha_1$/Ly-$\alpha_2$ in the laboratory frame, not in the emitter frame of the ion. Hence the laboratory angels have to be transformed correspondingly; the maximum of the distribution corresponds to an emitter angle of 90° in the ion frame; in the ion frame the emission pattern is symmetrical around 90°. A corresponding distribution is fitted to the data.

The anisotropy of the Ly-$\alpha_1$/Ly-$\alpha_2$ ratio has been investigated over a large energy region from 90 to 350 MeV/u for $U^{92+}\rightarrow N_2$ collisions in [14,17]. Here the Ly-$\alpha_1$/Ly-$\alpha_2$ ratio increases with decreasing ion energy. In [17] also a theoret-

TABLE I. Anisotropy $\beta_2$ and shape parameter $\mu$ (in brackets) for 90, 220, and 310 MeV/u $U^{92+}$-$N_2$ collisions for the angular distribution of the Ly-$\alpha_1$/Ly-$\alpha_2$ ratio. Experimental and theoretical results are compared, see also [14,17].

| Energy (MeV/u) | Experiment | Present theory | | Surzhykov *et al.* [17] | |
|---|---|---|---|---|---|
| | | $E1$ | $E1 \otimes M2$ | $E1$ | $E1 \otimes M2$ |
| 90 | −0.375 ±0.01 | −0.25 | −0.32 | −0.23 | −0.29 |
| | (1.90 ±0.1) | (1.49) | (1.71) | (1.45) | (1.61) |
| 220 | −0.225 ±0.02 | −0.18 | −0.23 | −0.17 | −0.22 |
| | (1.44 ±0.2) | (1.33) | (1.45) | (1.31) | (1.42) |
| 310 | −0.225 ±0.02 | −0.14 | −0.18 | −0.16 | −0.20 |
| | (1.44 ±0.2) | (1.24) | (1.33) | (1.29) | (1.38) |

ical description was given. Good agreement over the whole energy region was found after inclusion of retardation, i.e., of $M2$ transitions to the prevailing $E1$ decay of the $2p_{3/2}$ state. Neglecting the $M2$ transition amplitude will reduce the predicted anisotropy by about 20% in the whole energy range [17]. The important role of retardation effects in REC angular distribution was first noted in [18]. In the following, we will not consider this "$E1$-$M2$ interference" or multipole mixing explicitly.

Here, we will concentrate on the low energy region around 100 MeV/u and treat in our calculation below only the dominant $E1$ contribution. However, for comparison we will include the same enhancement factor into our final result. For completeness we give in Table I also the $\beta_2$ values reported in [14,17] for 90 and 220 MeV/u $U^{92+}$-$N_2$ collisions. Finally we include also the 310 MeV/u data shown in Fig. 3(a), despite that this energy is already beyond the validity of our theoretical approach. Moreover, we give the values $\mu$ for $f_{max}/f_{min}$ [see Eq. (15)] converted from $\beta_2$ according to Eq. (16). All values are additionally compared to the theory given in Ref. [17], both for pure $E1$ transition and inclusion $E1$-$M2$ interference. The results of our calculations are close to the one with pure $E1$ inclusion in Ref. [17]. Adding the coherence effects gives a corresponding accordance, where our results are slightly closer to the experimental values. Below in Fig. 4 a more detailed comparison of the different theories is given over an energy range between 80 and 230 MeV/u.

At the lowest energy of 90 MeV/u the observed anisotropy is larger than all the predictions. However, we note that this is probably caused by contributions from nonradiative capture starting to dominate REC at low ion energies and

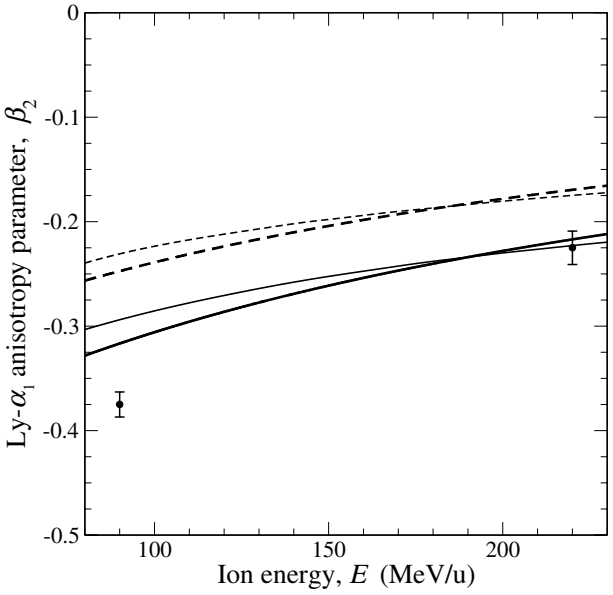


FIG. 4. Anisotropy parameter $\beta_2$ [cf., Eq. (5)] for the Ly-$\alpha_1$ emission as a function of ion energy (in the range between 80 and 230 MeV/u). The curves give our theoretical result (bold lines) in comparison to the calculations reported in the literature [15,16]. For the dashed lines only $E1$ transitions are considered, whereas the full lines comprise the enhancement factor due to the coherent inclusion of $M2$ amplitudes. The data points give the experimental values from [1] for the equivalent Ly-$\alpha_1$/Ly-$\alpha_2$ ratio.

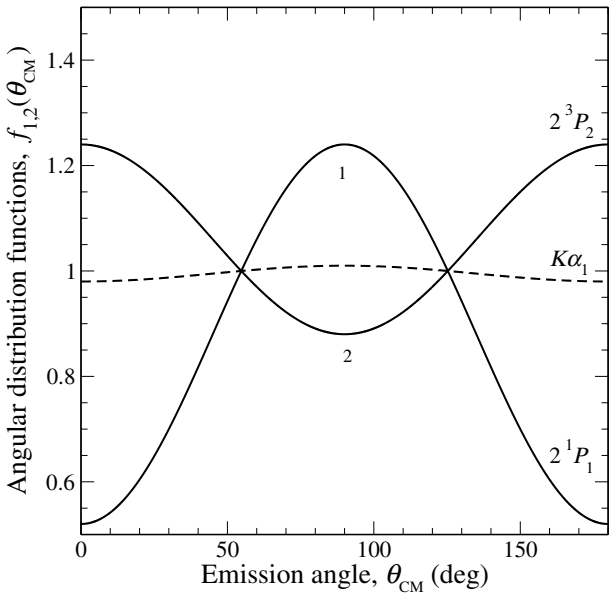


FIG. 5. The angular distribution functions $f_1(\theta_{c.m.})$ and $f_2(\theta_{c.m.})$ in the ion frame (c.m.) for the $K\alpha_1$ components, see Eqs. (76) and (90), associated with the $2\,^1P_1$ and $2\,^3P_2$ states, 1 and 2, respectively (for initially H-like $U^{91+}$ ions at 102 MeV/u). Additionally, the sum of both angular distributions for the composed $K\alpha_1$ emission, $f(\theta_{c.m.})$, see Eq. (97), is displayed (dashed line).

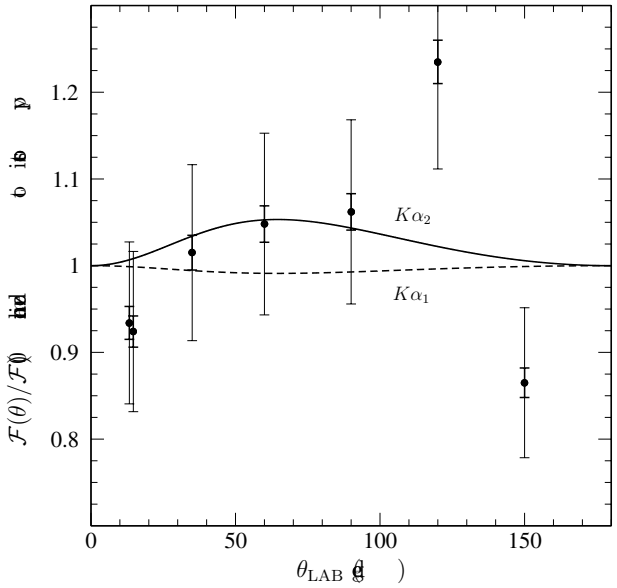


FIG. 6. The normalized to isotropy angular distributions $\mathcal{F}(\theta_{\text{laboratory}})/\mathcal{F}(0)$ in the laboratory frame are depicted for the $K\alpha_1$ and $K\alpha_2$ emission at $E=102$ MeV/u, see Eqs. (93) and (98), respectively. Additionally experimental data points from [2] are given for the $K\alpha_2$ emission characteristics (here large systematic inaccuracies apply beyond the given small statistical errors).

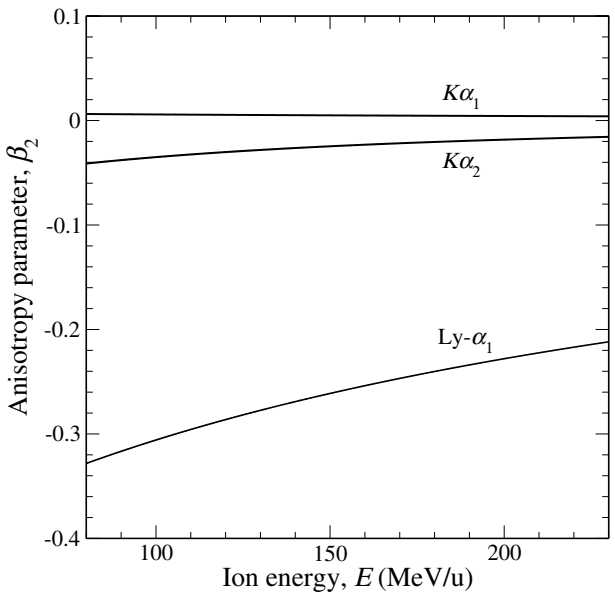


FIG. 7. The energy dependence of the anisotropy parameter $\beta_2$ for $K\alpha_{1,2}$ emission. For comparison, the anisotropy of the Ly-$\alpha_1$ emission for the initially bare ion case is shown additionally.

heavier targets. An overall good accordance between both the theories and the experimental results can be stated.

### C. $K\alpha_1/K\alpha_2$ intensity ratio for REC in $U^{91+}$

The KLL resonant transfer and excitation process was investigated for $U^{91+}$-$H_2$ collisions in [2]. Additionally at an off-resonance ion energy of 102 MeV/u the REC two-photon process was studied as a competing underlying process. The intensity ratio $K\alpha_1/K\alpha_2$ is plotted for that case in Fig. 3(b), showing within the experimental uncertainties practically an isotropic behavior (cf., straight line). Moreover, it was found that within the systematic uncertainties of the experiment of at least 10% the $K\alpha_2$ line emission was isotropic in the ion or emitter frame (cf., Fig. 5 in Ref. [2]). Our calculations are quite comparable with this and provide a small anisotropy for both the $K\alpha_1$ and $K\alpha_2$ line emission. In the shown representation also laboratory angles are given. The practically isotropic distribution displayed in this case, initially H-like ions, is in clear contrast to the strong anisotropy found for the initially bare ion case [Fig. 3(a)].

We emphasize that the direct REC process seems to a large extent be governed by the central force of the capturing nucleus and not by the presence of a spectator electron [12]. This is particularly true for the cross sections, where of course occupied levels have to be taken into account [13]. Similar statements seem to be true for the direct REC angular distributions [5,12]. However, the presence of a spectator electron has a crucial influence on the photon distribution. The capture is governed by the strength of the central ion field whereas the population of substates is governed in the intermediate state by the Pauli principle despite that the electron-electron interaction may be very weak in comparison.

This statement is also confirmed by the general considerations given in the calculations below. There, also an almost anisotropic behavior for the $K\alpha_1/K\alpha_2$ emission ratio in the considered case was found, for details see Figs. 5–8 below. In Fig. 8 the result of this calculation is displayed additionally and agrees reasonably well with the experimental finding. Moreover, the angular distributions for the two contributing transitions $2\,^1p_1 \rightarrow 1\,^1S_0$ and $2\,^3P_2 \rightarrow 1\,^1S_0$ are shown separately in Fig. 5. Both exhibit an appreciable anisotropy,

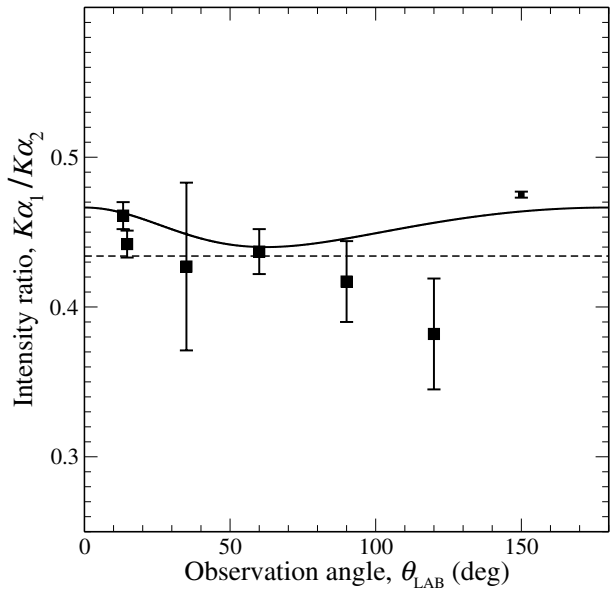


FIG. 8. Angular distribution for the $K\alpha_1/K\alpha_2$ intensity ratio as a function of the observation angle. The experimental data for 102 MeV/u $U^{91+} \rightarrow N_2$ collisions are shown for comparison [2].

however, with opposite signs, i.e., turned by 90° to each other, and thus mutually compensating in the total distribution shown for the $K\alpha_1$ radiation. There is also reasonable agreement with the $K\alpha_1$ emission characteristics can be stated.

## III. CAPTURE TO THE ELECTRONIC SHELL OF THE BARE NUCLEUS

### A. Emission of Ly-$\alpha$ photons

The amplitudes $A_{jm}$ [Eq. (7)] can be presented as

$$A_{jm} = (4\pi\alpha)^{1/2} \int \psi_K^*(\boldsymbol{r})(\boldsymbol{e}_2 \cdot \boldsymbol{\alpha})\psi_{jm}(\boldsymbol{r})e^{-i(\boldsymbol{k}_2\cdot\boldsymbol{r})}d^3r \quad (17)$$

with the electrons in $1s_{1/2}$ and $jm$ states described by relativistic Coulomb wave functions $\psi_K$ and $\psi_{jm}$. Here $\boldsymbol{e}_2$ and $\boldsymbol{\alpha}$ stand for the photon polarization vector and for the standard Dirac $\boldsymbol{\alpha}$-matrices, $\alpha=1/137$ is the fine structure constant.

The angular dependence of the amplitudes $A_{jm}$ can be obtained without specific calculations. The lower components of the Dirac bispinors can be presented in terms of the upper components and the Pauli $\sigma$-matrices. Thus the amplitudes $A_{jm}$ can be presented in terms of the upper components of the bispinors with the operator of the photon-electron interaction

$$\gamma(\boldsymbol{r}) = \frac{(4\pi\alpha)^{1/2}}{m}\left(-i(\boldsymbol{e}_2\cdot\boldsymbol{\nabla}_r) + \frac{1}{2}(\boldsymbol{\sigma}[\boldsymbol{e}_2\boldsymbol{\nabla}_r])\right). \quad (18)$$

It is instructive to present the amplitudes $A_{jm}$ in terms of the Fourier transformed functions $\psi^F$

$$A_{jm} = \int \psi_K^F(\boldsymbol{f}-\boldsymbol{k}_2)\gamma(\boldsymbol{f})\psi_{jm}^F(\boldsymbol{f})\frac{d^3f}{(2\pi)^3} \quad (19)$$

with

$$\gamma(\boldsymbol{f}) = \frac{(4\pi\alpha)^{1/2}}{m}\left((\boldsymbol{e}_2\boldsymbol{f}) + \frac{i}{2}(\boldsymbol{e}_2[\boldsymbol{\sigma}\boldsymbol{k}_2])\right). \quad (20)$$

We shall omit the upper index $F$ in further presentation.

We start with the emission of photons in $2p_j \to 1s$ decay: In our approach we include only $E1$ photons. The wave functions of $p$ states have the form

$$\psi_{jm}(\boldsymbol{f}) = \Phi_j(f)\Omega_{jm}(\boldsymbol{n}_f) \quad (21)$$

with the function $\Phi_j(f)$ depending only on $f=|\boldsymbol{f}|$, $\boldsymbol{n}_f=\boldsymbol{f}/f$, while

$$\Omega_{jm}(\boldsymbol{n}_f) = C^{jm}_{1m-1/2,1/2,1/2}Y_{1m-1/2}(\boldsymbol{n}_f)\varphi_{1/2} + C^{jm}_{1m+1/2,1/2,-1/2}Y_{1m+1/2}(\boldsymbol{n}_f)\varphi_{-1/2}. \quad (22)$$

Here $C^{jm}_{1a,1/2b}$ are the Clebsh-Gordan coefficients. The spherical harmonics $Y_{1a}$ can be presented as

$$Y_{1a}(\boldsymbol{n}) = \left(\frac{3}{4\pi}\right)^{1/2}(\boldsymbol{\varepsilon}_a\boldsymbol{n}), \quad a=0,\pm 1, \quad (23)$$

where the unit vectors

$$\boldsymbol{\varepsilon}_0 = \boldsymbol{\varepsilon}_z; \quad \boldsymbol{\varepsilon}_{\pm 1} = \mp\frac{1}{\sqrt{2}}(\boldsymbol{\varepsilon}_x \pm i\boldsymbol{\varepsilon}_y) \quad (24)$$

determine the reference frame, while $\varphi_{+1/2}=\binom{1}{0}$ and $\varphi_{-1/2}=\binom{0}{1}$ are the Pauli spinors with the definite values of the spin projection. In this notation

$$\psi_K(f) = \Phi_K(\boldsymbol{f})\varphi \quad (25)$$

with $\varphi$ standing for the spinor of the final state $1s$ electron.

Introducing

$$\boldsymbol{\Omega}_{jm} = \sqrt{\frac{3}{4\pi}}(C^{jm}_{1m-1/2,1/1/2,1/2}\boldsymbol{\varepsilon}_{m-1/2}\varphi_{1/2} + C^{jm}_{1m+1/2,1/2,-1/2}\boldsymbol{\varepsilon}_{m+1/2}\varphi_{-1/2}) \quad (26)$$

we can present

$$\Omega_{jm}(\boldsymbol{n}_f) = (\boldsymbol{\Omega}_{jm}\boldsymbol{n}_f) \quad (27)$$

and thus $\psi_{jm}(\boldsymbol{f})=\Phi_j(f)(\boldsymbol{\Omega}_{jm}\boldsymbol{n}_f)$. The leading contribution to the amplitude $A_{jm}$ comes from the first term on the right-hand side (rhs) of Eq. (18)

$$A_{jm} = \frac{(4\pi\alpha)^{1/2}}{m}\int \varphi^*\Phi_K(|\boldsymbol{f}-\boldsymbol{k}_2|)\Phi_j(f)(\boldsymbol{e}_2\cdot\boldsymbol{f})(\boldsymbol{\Omega}_{jm}\cdot\boldsymbol{n}_f)\frac{d^3f}{(2\pi)^3}, \quad (28)$$

corresponding to $E1$ transitions. Due to the transverse polarization of photons $(\boldsymbol{e}_2\cdot\boldsymbol{k}_2)=0$ we find

$$A_{jm} = \varphi^*(\boldsymbol{e}_2\cdot\boldsymbol{\Omega}_{jm})Q_j(\omega_2). \quad (29)$$

The particular form of the function $Q_j(\omega_2)$ is not important in our approach. Note also that in the lowest orders of expansion in powers of $\left(\frac{\alpha Z}{2}\right)^2$ the radial part of the wave function, i.e., the function $\Phi_j$ on the rhs of Eq. (21) is the same for both $j=1/2$ and $j=3/2$. We employ this approximation. Hence the functions $Q_j$ on the rhs of Eq. (29) do not depend on $j$, and we put

$$Q_j(\omega_2) = Q(\omega_2).$$

In the case of $j=3/2$ there are also $M2$ transitions caused by the second term of the expression (20) for the electron-photon interaction. Strictly speaking, it should be included together with the $k_1^2/p^2$ corrections to the $E1$ decay.

Emission of $M1$ photons in $2s_{1/2} \to 1s_{1/2}$ electron transitions can be treated in a similar way. The wave function for the $2s_{1/2}$ state is

$$\psi_{sm}(f) = \Phi_s(f)\varphi_m \quad (30)$$

with $\varphi_m$ being the spinor of the $2s$ state. The amplitude of the radiation can be presented as

$$A_{sm} = -\frac{i}{2}\varphi^*(\boldsymbol{\sigma}\cdot\boldsymbol{h})\varphi_m Q^s(\omega_2) \quad (31)$$

with

$$\boldsymbol{h} = [\boldsymbol{e}_2\cdot\boldsymbol{n}_2], \quad (32)$$

while $\boldsymbol{n}_2=\boldsymbol{k}_2/k_2$.

### B. Emission of the first photon

The angular structure of the corresponding amplitude

$$B_{jm} = (4\pi\alpha)^{1/2} \int \psi^*_{jm}(\boldsymbol{f}-\boldsymbol{k}_1)(\boldsymbol{e}_1\cdot\boldsymbol{\alpha})\psi_i(\boldsymbol{f})\frac{d^3f}{(2\pi)^3} \quad (33)$$

is more complicated since there is one more vector, i.e., the momentum of the initial electron $\boldsymbol{p}$.

Here we start with the intermediate $p$ state: except the contribution proportional to $(\boldsymbol{e}_1\cdot\boldsymbol{\Omega}_{jm})$ there are those containing the factors $(\boldsymbol{e}_1\cdot\boldsymbol{n}_p)(\boldsymbol{n}_p\cdot\boldsymbol{\Omega}_{jm})$ and $(\boldsymbol{e}_1\cdot\boldsymbol{n}_p)(\boldsymbol{k}_1\cdot\boldsymbol{\Omega}_{jm})$ with $\boldsymbol{n}_p=\boldsymbol{p}/p$. The latter one can be neglected in our approach, contributing values of the order $k_1^2/p^2$ after integration over the solid angle. Assuming that the axis $z$ runs along momentum $\boldsymbol{p}$, we shall find the amplitude $B_{jm}$ as the sum of the contributions proportional to $(\boldsymbol{e}_{1z}\cdot\boldsymbol{\Omega}_{jm})$ and $(\boldsymbol{e}_{1t}\cdot\boldsymbol{\Omega}_{jm})$ with the lower index "$t$" denoting the vector in the $xy$ plane. Thus the amplitude can be presented as

$$B_{jm} = (4\pi\alpha)^{1/2}\sqrt{\frac{4\pi}{3}}T(p)[(\boldsymbol{e}_{1t}\cdot\boldsymbol{\Omega}^*_{jm}) + \lambda(p)(\boldsymbol{e}_{1z}\cdot\boldsymbol{\Omega}^*_{jm})]\varphi_i, \quad (34)$$

with $\varphi_i$ being the Pauli spinor of the incoming electron while $T(p)$ and $\lambda(p)$ are certain functions of the incoming continuum electron momentum $p$—see Appendix A.

For the calculation of the angular distributions we shall need only the function $\lambda(p)$. We shall use the relativistic Coulomb functions in the form suggested in [19], where they are presented in terms of a certain operator $\hat{\Gamma}$ acting on the nonrelativistic wave functions $\psi^{nr}(\boldsymbol{f})$

$$\psi(\boldsymbol{f}) = \hat{\Gamma}\psi^{nr}(\boldsymbol{f}) \quad (35)$$

with

$$\hat{\Gamma} = 1 + \frac{(\boldsymbol{\alpha}\cdot\boldsymbol{f})}{2m} + \hat{\Gamma}_r. \quad (36)$$

If the operator $\hat{\Gamma}_r$ is neglected, the functions (35) are the Darwin [20] and Furry-Sommerfeld-Maue functions [21,22] for the bound and continuum electron states correspondingly, see, e.g., [23]. The second term on the rhs of Eq. (36) generates the nonzero values of the lower components of the Dirac bispinors, while the operator of the electromagnetic interaction $(\boldsymbol{e}\cdot\boldsymbol{\alpha})$ contracts the lower and upper components of the two-electron states. The operator $\hat{\Gamma}_r$ generates the higher order relativistic corrections to each of them. For the $2p$ states they are of the order $\frac{1}{2}(\frac{\alpha Z}{2})^2$, while for the continuum electrons they are of the order $\varepsilon/m$ [24,25]. In both cases they do not exceed 10%, and will be neglected. Note that in this approximation the function $T(p)$ does not depend on $j$.

The straightforward calculation, with the details presented in Appendix A, provides

$$\lambda(p) = -\frac{p-3i\eta_2}{p-i\eta_2} \quad (37)$$

with $\eta_2=m\alpha Z/2$. The differential cross sections will actually contain the value

$$|\lambda(p)|^2 = 1 + \frac{8\xi^2}{4+\xi^2} \quad (38)$$

with

$$\xi = \frac{m\alpha Z}{p}. \quad (39)$$

We shall denote $\lambda^2=|\lambda(p)|^2$. It will be convenient also to present the results in terms of the parameter

$$\Lambda = \lambda^2 - 1 = \frac{8\eta_1^2}{4p^2+\eta_1^2}, \quad (40)$$

with $\eta_1=m\alpha Z$. While $\lambda^2$ describes the relative weights of the longitudinal and transverse polarizations of the photon with respect to the direction of the electron momenta in capture to a $p$ state; $\Lambda$ describes the excess of the longitudinal polarization over the transversely polarized contribution in the same process. As one can see from Eq. (40), the anisotropy effects die away with the energy growth.

In the case of intermediate $s$ states the structure of the amplitude is simpler, since the angular dependence is contained in the factor $(\boldsymbol{e}_1\cdot\boldsymbol{n}_p)$. The amplitude can be presented as

$$B_{sm} = T^s(p)e_{1z}\varphi^*_m\varphi, \quad (41)$$

with the explicit form of $T^s(p)$ being given in Appendix A.

### C. Angular distribution

#### 1. Shape of $t_2^2$ dependence

The shape of the $t_2$ dependence for the angular distribution of the Ly-$\alpha_1$/Ly-$\alpha_2$ ratio can be obtained by the analysis of the dependence of the angular part of the amplitude, without particular calculations of the radial part. This can be done by using the properties of the spherical spinors, which are contained in the factors $A_{jm}$ and $B_{jm}$ on the rhs of Eq. (6). The spherical spinors enter this equation in terms of the sums [26]

$$\sum_m \Omega_{jm}(\mathbf{a})\Omega^*_{jm}(\mathbf{b}) = (\mathbf{a}\cdot\mathbf{b}) + i(\boldsymbol{\sigma}[\mathbf{a}\cdot\mathbf{b}]) \quad (42)$$

for $j=1/2$, and

$$\sum_m \Omega_{jm}(\mathbf{a})\Omega^*_{jm}(\mathbf{b}) = 2(\mathbf{a}\cdot\mathbf{b}) - i(\boldsymbol{\sigma}[\mathbf{a}\cdot\mathbf{b}]) \quad (43)$$

for $j=3/2$. These equations are true for any three-dimensional vectors $\mathbf{a}$ and $\mathbf{b}$.

In the case of the intermediate state $2p_{1/2}$ we expect an isotropic distribution for the second photon, since the probabilities to occupy the intermediate states with $m=\pm 1/2$ are the same, while the interference is killed by integration over $\Omega_1$. With the technique developed above we find

$$\frac{d\sigma}{dt_1 dt_2} = |(\boldsymbol{e}_2 \cdot \boldsymbol{e}_{1t}) + i(\boldsymbol{\sigma}[\boldsymbol{e}_2 \cdot \boldsymbol{e}_{1t}])|^2 + \lambda^2 |(\boldsymbol{e}_2 \cdot \boldsymbol{e}_{1z}) + i(\boldsymbol{\sigma}[\boldsymbol{e}_2 \cdot \boldsymbol{e}_{1z}])|^2 C_1(p). \quad (44)$$

The explicit form of the function $C_1(p)$ will not be important for the shape of the distribution. Since $|(\mathbf{a}\cdot\mathbf{b})+i(\boldsymbol{\sigma}[\mathbf{a}\cdot\mathbf{b}])|^2 = (\mathbf{a}\cdot\mathbf{b})^2+([\mathbf{a}\cdot\mathbf{b}])^2 = a^2b^2$, Eq. (44) can be presented as

$$\frac{d\sigma}{dt_1 dt_2} = (e_{1t}^2 + \lambda^2 e_{1z}^2) C_1(p)^2. \quad (45)$$

The rhs does not depend on $t_2$ indeed for any value of the energy of the captured electron. Also, for the transition via the $2s_{1/2}$ state the angular distribution of the second $M1$ photon is isotropic. Thus the angular distribution of the total Ly-$\alpha_2$ line is isotropic, what was always assumed.

For the intermediate $2p_{3/2}$ state the angular distribution can be presented as

$$\frac{d\sigma}{dt_1 d\Omega_2} = \{e_{1t}^2 + 3(\boldsymbol{e}_{1t}\cdot\boldsymbol{e}_2)^2 + \lambda^2[e_{1z}^2 + 3(\boldsymbol{e}_{1z}\cdot\boldsymbol{e}_2)^2]\}\frac{C_2(p)}{2\pi}. \quad (46)$$

As above, the explicit form of the function $C_2(p)$ will not be important for the shape of the distribution. Summing over the photon polarizations $\nu$ by using the well-known formula

$$\Sigma_\nu (e)_i^{*\nu} (e)_j^\nu = \delta_{ij} - n_i n_j$$

with $\boldsymbol{n}$ being the unit vector directed along the momentum of the corresponding photon, and carrying out the integration over $t_1$, we find

$$R(t_2) = \left[4 + \frac{5\Lambda}{3} - \Lambda t_2^2\right] C(p). \quad (47)$$

Recall that in this section we do not determine the function $C(p)$, but find only the shape of the distribution curve. For the shape parameter $\mu$ defined by Eq. (15) we find

$$\mu = \frac{12+5\Lambda}{12+2\Lambda}. \quad (48)$$

For the specific conditions of the experiment with an energy of the captured electron of about $\varepsilon = 50$ keV, we obtain

$$\lambda^2 = 3.92, \quad (49)$$

and thus the functions $f_j(t)$ introduced by Eq. (9) are

$$f_{1/2}(t_2) = 1; \quad f_{3/2}(t_2) = 1.11 - 0.33 t_2^2; \quad \mu = \frac{f_{3/2}(0)}{f_{3/2}(1)} = 1.49,$$

see also Table I.

The anisotropy parameter is

$$\beta_2 = \frac{-\Lambda}{2(\Lambda+3)}. \quad (50)$$

Using Eq. (40) we can find its energy dependence $\beta_2(E)$. In Fig. 4 we compare our results for the anisotropy parameter $\beta_2(E)$ with the calculations presented in Ref. [17]—both including and excluding $M2$ transitions; the two available experimental data points are also shown for comparison. Our result coincides with the pure $E1$ result of [17], giving evidence for the validity of both the approaches.

For the high energy $\varepsilon = 170$ keV [corresponding to projectile energy $E = 310$ MeV/u, cf. Fig. 3(a)] we find $\lambda^2 = 2.16$. This leads to $\mu = 1.24$. Note, however, that in the framework of our approach this is rather an estimation. More sophisticated analysis at such high energies requires a consistent inclusion of relativistic effects.

It is instructive to present the square of the amplitude (8) as

$$|F_j|^2 = \frac{\sum_m |A_{jm}|^2 |B_{jm}|^2}{(\varepsilon_f + \omega_2 - \varepsilon_j)^2 + \Gamma_j^2/4}. \quad (51)$$

We omit the modulus sign through the paper. Summation over the photon polarizations is assumed to be carried out. The interference terms containing the products $A_{jm}B_{jm'}$ with $m \neq m'$ vanish either due to orthogonality of the spin functions or after integration over the azimuthal angle of the first photon. Using the equations presented in Appendix A we find

$$B_{3/21/2}^2 = C_1^2(p)\frac{1+t_1^2}{2}; \quad (52)$$

$$B_{3/23/2}^2 = C_1^2(p)\left[\frac{2(1-t_1^2)\lambda^2}{3} + \frac{1+t_1^2}{6}\right].$$

We define

$$D_m = \int dt_1 B_{jm}^2 \quad (53)$$

omitting the index, labeling the angular momentum $j$. The angular dependence of the square of the amplitude, presented by Eq. (51), is thus determined by the sum

$$y(t_2) = \sum_m A_{jm}^2(t_2) D_m.$$

If all the coefficients $D_m$ have the same value $D_m = D$, the function $y(t_2)$ does not depend on $t_2$, since $\Sigma A_{jm}^2(t_2)$ does not depend on $t_2$. Hence the deviation between the values of $D_m$ leads to the actual dependence on $t_2$ (anisotropy). Defining also

$$d_m = \frac{D_m}{\sum_m D_m} \quad (54)$$

we find

$$d_{1/2} = \frac{\lambda^2 + \frac{1}{2}}{2(2+\lambda^2)}; \quad d_{3/2} = \frac{3}{4(2+\lambda^2)}, \quad (55)$$

while the alignment parameter $\mathcal{A}_2 = (d_{3/2} - d_{1/2})/(d_{3/2} + d_{1/2})$ is

$$\mathcal{A}_2 = \frac{-\Lambda}{\Lambda+3}. \quad (56)$$

Hence we have $\mathcal{A}_2=2\beta_2$, in agreement with [17,27], and the energy dependence of the alignment parameter can also be read from Fig. 4.

#### 2. Ly-$\alpha_1$/Ly-$\alpha_2$ *intensity ratio*

Now we calculate the angular distributions $\frac{d\sigma}{dt_2}$ for both Ly-$\alpha_1$ and Ly-$\alpha_2$ emission. Using Eq. (51) for the square of the amplitude we obtain

$$\frac{d\sigma_x}{dt_1 dt_2} = \sum_m \frac{\omega_1 A_{xm}^2(t_2)}{4\pi} \int \frac{\omega_2 B_{xm}^2(t_1)}{4\pi\cdot 2} \frac{d\omega_2}{|\omega_2 - \varepsilon_x + \varepsilon_f + i\Gamma_x/2|^2}, \tag{57}$$

with $x$ standing for $2p_{1/2}$ and $2s_{1/2}$ states (Ly-$\alpha_2$ line) or the $2p_{3/2}$ state (Ly-$\alpha_1$ line).

Using the formulas, presented in Appendix A, we obtain

$$\frac{d\sigma_{2p_{3/2}}}{dt_2} = X(p)\left(4 + \frac{5\Lambda}{3} - \Lambda t_2^2\right); \quad \frac{d\sigma_{2p_{1/2}}}{dt_2} = 2X(p)\left(1 + \frac{\Lambda}{3}\right);$$

$$\frac{d\sigma_{2s_{1/2}}}{dt_2} = 8X(p)(1+\xi^{-2}) \tag{58}$$

with $\xi$ defined by Eq. (39), while

$$X(p) = \frac{\alpha(2\pi\alpha Z)^2}{3a(p)^2}\eta_1^5\omega_1\xi V(p)^2, \tag{59}$$

with $V(p)$ defined by Eq. (A8).

For the angular distribution of the Ly-$\alpha_1$/Ly-$\alpha_2$ ratio we find

$$R(t_2) = \frac{12 + 5\Lambda - 3\Lambda t_2^2}{2(15 + \Lambda + 12\xi^{-2})}. \tag{60}$$

It was shown in [17] that interference between $E1$ and $M2$ transitions provides noticeable contribution to the anisotropy effects in the Ly-$\alpha_1$ line. The energy dependence of the anisotropy parameter $\beta_2(E)$ is not altered, but the transition is described by the effective parameter

$$\beta_2^{eff}(E) = a\beta_2(E),$$

while the coefficient $a$ does not depend on the energy $E$ of the colliding particles. The calculations [17] provided $a=1.28$. This factor for multipole mixing has to be taken into account on top of our result.

Including this factor, our final result at low energy ($E=90$ MeV/u) fits the experimental data even better than the previous calculations. For the energy $E=310$ MeV/u our results are less accurate since the relativistic effects in the dynamics of the incoming electron become important. Inclusion of $E1$-$M2$ interference shifts the value of $\mu$ from 1.24 to 1.33, i.e., closer to the experimental value $\mu=1.44$. However, the absolute values of the ratio still make only 2/3 of the experimental value. This is in agreement with the estimation of errors of our approach for these energies.

For the particular Ly-$\alpha$ lines our results also agree with the previous ones. The Ly-$\alpha_2$ line is isotropic, as well as in the previous experimental and theoretical results. The energy dependence of the anisotropy parameter for the Ly-$\alpha_1$ line is shown in Fig. 4.

## IV. CAPTURE BY THE SINGLE-ELECTRON ION

### A. Emission of $K\alpha_1$ photons

In the following we turn to the case when the electron is captured to the $K$ shell of the ion $U^{91+}$ which already has one electron in the $1s_{1/2}$ state. The final state is described by the function

$$\Psi_K(\boldsymbol{r}_1,\boldsymbol{r}_2) = \psi_K(r_1)\psi_K(r_2)\kappa(0,0) \tag{61}$$

with $\kappa(s,s_z)$ denoting the two-electron spin function with the total spin $s$ and its projection $s_z$. The intermediate state electron wave functions are built according to the $j$-$j$ coupling scheme

$$\begin{aligned}\Psi_{JM}(r_1,r_2) = {}& \Phi_{3/2}(r_1)\Phi_K(r_2) \\ & \times[C^{JM}_{3/2M-1/2,1/2,1/2}\Omega_{3/2,M-1/2}(\boldsymbol{n}^1)\chi_{1/2,1/2} \\ & + C^{JM}_{3/2M+1/2,1/2,-1/2}\Omega_{3/2,M+1/2}(\boldsymbol{n}^1)\chi_{1/2,-1/2}] \\ & - (\boldsymbol{r}_1,\sigma_1 \rightleftharpoons \boldsymbol{r}_2,\sigma_2)\end{aligned} \tag{62}$$

with $\boldsymbol{n}^1=\boldsymbol{r}_1/r_1$, $\chi$ is the Pauli spinor of the $1s_{1/2}$ electron, while $\sigma_{1,2}$ stands for the spin variables.

Being expressed in terms of the spin functions $\kappa(s,s_z)$ the wave functions for $J=1$ are

$$\begin{aligned}\Psi_{10}(\boldsymbol{r}_1,\boldsymbol{r}_2) = {}& \frac{1}{\sqrt{3}}[\Phi_{3/2}(r_1)\Phi_K(r_2)Y_{10}(\boldsymbol{n}^1) + (\boldsymbol{r}_1 \rightleftharpoons \boldsymbol{r}_2)]\kappa(0,0) \\ & + \frac{1}{2\sqrt{3}}[\Phi_{3/2}(r_1)\Phi_K(r_2)Y_{11}(\boldsymbol{n}^1) \\ & - (\boldsymbol{r}_1 \rightleftharpoons \boldsymbol{r}_2)]\kappa(1,-1) \\ & - \frac{1}{2\sqrt{3}}[\Phi_{3/2}(r_1)\Phi_K(r_2)Y_{1,-1}(\boldsymbol{n}^1) \\ & - (\boldsymbol{r}_1 \rightleftharpoons \boldsymbol{r}_2)]\kappa(1,1)\end{aligned} \tag{63}$$

for $M=0$, and

$$\begin{aligned}\Psi_{1M}(\boldsymbol{r}_1,\boldsymbol{r}_2) = {}& \frac{1}{\sqrt{3}}[\Phi_{3/2}(r_1)\Phi_K(r_2)Y_{1M}(\boldsymbol{n}^1) \\ & + (\boldsymbol{r}_1 \rightleftharpoons \boldsymbol{r}_2)]\kappa(0,0) \\ & + \frac{M}{2\sqrt{3}}[\Phi_{3/2}(r_1)\Phi_K(r_2)Y_{1M}(\boldsymbol{n}^1) \\ & - (\boldsymbol{r}_1 \rightleftharpoons \boldsymbol{r}_2)]\kappa(1,0) \\ & - \frac{M}{2\sqrt{3}}[\Phi_{3/2}(r_1)\Phi_K(r_2)Y_{10}(\boldsymbol{n}^1) \\ & - (\boldsymbol{r}_1 \rightleftharpoons \boldsymbol{r}_2)]\kappa(1,M)\end{aligned} \tag{64}$$

for the values of the projection $M=\pm 1$.

For $J=2$ the total spin of the two-electron system has a definite value $s=1$. The wave functions are

$$\Psi_{20}(\boldsymbol{r}_1,\boldsymbol{r}_2)=\frac{1}{\sqrt{3}}[\Phi_{3/2}(r_1)\Phi_K(r_2)Y_{10}(\boldsymbol{n}^1)-(\boldsymbol{r}_1\rightleftharpoons\boldsymbol{r}_2)]\times\kappa(1,0)+\frac{1}{2\sqrt{3}}[\Phi_{3/2}(r_1)\Phi_K(r_2)Y_{11}(\boldsymbol{n}^1)-(\boldsymbol{r}_1\rightleftharpoons\boldsymbol{r}_2)]\times\kappa(1,-1)+\frac{1}{2\sqrt{3}}[\Phi_{3/2}(r_1)\Phi_K(r_2)Y_{1-1}(\boldsymbol{n}^1)-(\boldsymbol{r}_1\rightleftharpoons\boldsymbol{r}_2)]\kappa(1,1) \quad (65)$$

for $M=0$, while

$$\Psi_{2M}(r_1,r_2)=\frac{1}{2}[\Phi_{3/2}(r_1)\Phi_K(r_2)Y_{1M}(\boldsymbol{n}^1)-(\boldsymbol{r}_1\rightleftharpoons\boldsymbol{r}_2)]\times\kappa(1,0)+\frac{1}{2}[\Phi_{3/2}(r_1)\Phi_K(r_2)Y_{10}(\boldsymbol{n}^1)-(\boldsymbol{r}_1\rightleftharpoons\boldsymbol{r}_2)]\times\kappa(1,M) \quad (66)$$

for $M=\pm1$, and

$$\Psi_{2M}(r_1,r_2)=\frac{1}{\sqrt{2}}[\Phi_{3/2}(r_1)\Phi_K(r_2)Y_{1M'}(\boldsymbol{n}^1)-(\boldsymbol{r}_1\rightleftharpoons\boldsymbol{r}_2)]\kappa(1,M') \quad (67)$$

for $M=\pm2$, with $M'=M/2$

The amplitudes $A_{JM}$ are determined by Eq. (7) with the operator $\gamma^{(2)}=\gamma(\boldsymbol{r}_1)+\gamma(\boldsymbol{r}_2)$ with $\gamma(\boldsymbol{r}_i)$ determined by Eq. (20).

### B. Summation over $M$

Following the procedure developed in the previous section we present the amplitudes $A_{JM}$ in terms of the functions $Y_{10}(\boldsymbol{e}_2)=\left(\frac{3}{4\pi}\right)^{1/2}\boldsymbol{e}_{2z}$ and $Y_{1\pm1}(\boldsymbol{e}_2)=\left(\frac{3}{4\pi}\right)^{1/2}(\boldsymbol{e}_2)_{\pm1}$. In a similar way the amplitudes $B_{JM}$ are presented in terms of the components $e_{1z}$ and $e_{1t}$ with the relative weights determined by the function $\lambda(p)$ introduced by Eq. (34).

For the calculation of the angular distribution of the second photon $d\sigma/dt_2$ we can put

$$|F_J|^2=\frac{\sum_M A_{JM}^2B_{JM}^2}{(\varepsilon_f+\omega_2-\varepsilon_J)^2+\Gamma_J^2/4}. \quad (68)$$

The interference terms containing the products $A_{JM}B_{JM'}$ with $M\neq M'$ vanish either due to orthogonality of the spin functions or after the integration over the solid angle of the first photon.

### C. Intermediate state $[1s_{1/2},2p_{3/2}]_1$: $2\,^1P_1$

In this case the $K\alpha_1$ photon is emitted by an $E1$ transition. Hence the spin variables are not touched, and only the first terms on the rhs of Eqs. (38) and (39) contribute to the amplitudes $A_{1M}$. The latter can be presented as

$$A_{1M}=e_{2M}S(\omega_2). \quad (69)$$

The specific form of the function $S(\omega_2)$ is not important for us here. The angular distribution of the photons emitted in the decay of the state $1M$ is thus

$$\frac{dW_M}{dt_2}=e_{2M}^2\frac{S(\omega_2)^2\omega_2}{4\pi} \quad (70)$$

with the sum over the photon polarizations being carried out. Introducing

$$q_M=\sum_\nu \boldsymbol{e}_{2M}^{\nu*}\boldsymbol{e}_{2M}^{\nu},$$

with $\nu$ standing for the photon polarizations, we obtain $q_0=1-t_2^2$, $q_1=q_{-1}=\frac{1+t_2^2}{2}$. Of course, the probabilities $W_M$ do not depend on $M$, being

$$W_M=\frac{1}{3}\frac{S(\omega_2)^2\omega_2}{\pi}. \quad (71)$$

In the two-photon decay the weights of the contributions $A_{1M}^2$ are determined by the values $B_{1M}^2$—Eq. (33). The angular distribution of the two photons is

$$\frac{d\sigma}{dt_1dt_2}=\sum_M\frac{B_{1M}^2e_{2M}^2\omega_1}{4\times(2\pi)^3}\int\frac{S(\omega_2)^2\omega_2d\omega_2}{(\omega_2-\varepsilon_\gamma)^2+\Gamma_1^2/4}, \quad (72)$$

with $\varepsilon_\gamma$ standing for the difference of the binding energy of $2\,^1P_1$ and $1\,^1S_0$ states. Since we neglect all the other channels of the decay of the $2\,^1P_1$ state we put $\Gamma_1=W_M$ in the standard Breit-Wigner integral on the rhs of Eq. (47). Thus

$$\frac{d\sigma}{dt_1dt_2}=\frac{3\omega_1}{16\pi}\sum_M B_{1M}^2g_M. \quad (73)$$

The weights of the contributions $g_M$

$$B_{10}^2=\frac{2}{3}(1-t_1^2)\lambda^2T(p);$$

$$B_{1\pm1}^2=\frac{1}{3}(1+t_1^2)T(p) \quad (74)$$

can be obtained by using Eqs. (63) and (64). The specific form of the function $T(p)$ is not important for the calculation of the shape of the angular distributions.

Averaging over the polarizations of the initial two-electron state we find

$$\frac{d\sigma}{dt_2}\frac{\alpha2\omega_1T(p)^2}{3}[1+\lambda^2-t_2^2(\lambda^2-1)]. \quad (75)$$

At $\lambda^2=3.92$—see Eq. (49)—this leads for the $2\,^1P_1$ decay to

$$f_1(t_2)=1.24-0.72t_2^2;\quad \frac{f_1(0)}{f_1(1)}=2.4. \quad (76)$$

One can see the anisotropy to be larger than in the decay of the single-electron $2p_{3/2}$ state.

For a more detailed analysis we introduce

$$D_{JM} = \int dt_1 B_{JM}^2. \tag{77}$$

The anisotropy is due to the dependence of $D_{JM}$ on $M$. We introduce also

$$d_{JM} = \frac{D_{JM}}{\sum_M D_{JM}} \tag{78}$$

and find

$$d_{10} = \frac{\lambda^2}{2+\lambda^2}; \quad d_{1\pm1} = \frac{1}{\lambda^2+2}. \tag{79}$$

### D. Intermediate state $[1s_{1/2}, 2p_{3/2}]_2$: $2\,^3P_2$

In this case the $K\alpha_1$ photon is emitted as $M2$ transition. It takes place due to the spin-dependent term of the operator $\gamma$ presented by Eq. (20). The amplitudes $A_{2M}$ of the radiation of the second photon can be presented as

$$A_{2M} = a_{2M}\tilde{S}(\omega_2) \tag{80}$$

with

$$a_{20} = \sqrt{3}n_{kz}h_z; \quad a_{2\pm1} = (n_{kz}h_{\pm1} + h_z n_{k\pm1}); \quad a_{2\pm2} = \sqrt{2}n_{k\pm1}h_{\pm1}, \tag{81}$$

while the vector $\boldsymbol{h}$ is determined by Eq. (32).

The angular distribution of the photon emitted in the decay of the state with the projection $M$ of the angular momentum is

$$\frac{dW_M}{dt_2} = a_{2M}^2 \frac{\tilde{S}(\omega_2)^2\omega_2}{4\pi}, \tag{82}$$

see Eq. (80). Summing over the polarizations of the photon we obtain

$$a_{20}^2 = 3t_2^2(1-t_2^2); \quad a_{2-1}^2 + a_{21}^2 = 4t_2^4 - 3t_2^2 + 1; \tag{83}$$

$$a_{2-2}^2 + a_{22}^2 = 1 - t_2^4.$$

As well as in the previous case

$$\frac{d\sigma}{dt_1 dt_2} = \sum_M \frac{B_{2M}^2 a_{2M}^2 \omega_1}{4\cdot(2\pi)^3} \int \frac{\tilde{S}(\omega_2)^2\omega_2 d\omega_2}{(\omega_2 - \varepsilon_\gamma)^2 + \Gamma_2^2/4}. \tag{84}$$

Except for the transition to the ground state $1\,^1S_0$, the level $2\,^3P_2$ can also decay to the state $2\,^3S_1$. Thus the probability $W_{1S}$ of the transition to the $1S$ state is smaller than the total width $\Gamma_T$ of the level

$$\frac{W_{1S}}{\Gamma_T} = c < 1. \tag{85}$$

We shall determine the value of $c$ at the end of this section. Thus

$$\frac{d\sigma}{dt_1 dt_2} = \frac{\alpha\cdot 5\omega_1}{4} \sum_M B_{2M}^2 a_{2M}^2 c \tag{86}$$

with

$$B_{20}^2 = \frac{1}{3}\left[2(1-t_1^2)\lambda^2 + \frac{1}{2}(1+t_1^2)\right]T(p)^2;$$

$$B_{2\pm1}^2 = \frac{1}{2}\left[(1-t_1^2)\lambda^2 + \frac{1}{2}(1+t_1^2)\right]T(p)^2;$$

$$B_{2\pm2}^2 = \frac{1}{2}(1+t_1^2)T(p)^2. \tag{87}$$

The function $T(p)$ is the same as in Eq. (74).

After the integration over $t_1$ we obtain

$$\frac{d\sigma}{dt_2} = \frac{\alpha\cdot 5\omega_1}{2} T(p)^2 c\left(1 + \frac{\lambda^2}{3} + t_2^2\frac{\lambda^2-1}{3}\right). \tag{88}$$

It is amusing that the terms containing $t_2^4$ cancel out. Due to this cancellation the distribution obtains its smallest value at $t_2=0$, corresponding to the angle $\theta_{\text{c.m.}}=90°$. Parameters $d_{2M}$ defined by Eq. (78) are

$$d_{20} = \frac{1}{5}\frac{1+2\lambda^2}{2+\lambda^2}; \quad d_{2\pm1} = \frac{3}{10}\frac{1+\lambda^2}{2+\lambda^2}; \quad d_{2\pm2} = \frac{3}{5}\frac{1}{2+\lambda^2}. \tag{89}$$

At $\lambda^2=3.92$, Eq. (49), we find for the asymmetry function (9) for the $2\,^3P_2$ decay

$$f_2(t_2) = 0.88 + 0.36t_2^2; \quad \frac{f_2(0)}{f_2(1)} = 0.71. \tag{90}$$

In order to find the angular distribution of the $K\alpha_1$ transition, we must determine the value of

$$c = \frac{W_{1S}}{W_{1S} + W_{2S}}, \tag{91}$$

with $W_{1S}$ and $W_{2S}$ being the probabilities of decays to $1\,^1S_0$ and $2\,^3S_1$ states, respectively. Considering transitions to $2S$ states it is sufficient to include only the $E1$ one to $2\,^3S_1$, since the $M2$ transition to the state $2\,^1S_0$ is suppressed. The probability of a transition to the $2\,^3S_1$ state contains an additional factor $\left(\frac{\alpha Z}{2}\right)^2$, compared to the probability of a transition to the $1\,^1S_0$ state. Hence the former transition should be included together with higher relativistic corrections to the latter one. Strictly speaking, in our approximation we must neglect the transition to the state $2\,^3S_1$, just putting $c=1$. However, using the functions (35) we obtain

$$W_{1S} = \frac{\alpha}{5}\left(\frac{8}{9}\right)^5 \frac{\omega_{1S}^5}{\eta_1^2 m^2}; \quad W_{2S} = \frac{12\alpha\omega_{2S}^3}{\eta_1^2}, \tag{92}$$

with $\eta_1 = m\alpha Z$. Here $\omega_{1S,2S}$ are the differences between the energies of these states and that of the $2\,^3P_2$ state. Assuming the nonrelativistic Coulomb value for the energy $\omega_{1S}$ and the $LS$ Coulomb splitting value for $\omega_{2S}$ ($\omega_{2S}=0$ in nonrelativistic approximation), we find $c=0.83$. A more rigorous GRASP [28] calculation leads to $c=0.70$. The noticeable magnitude of $1-c$ can be viewed as the result of multiplying the small parameter $\left(\frac{\alpha Z}{2}\right)^2$ by a numerically large factor. In order to be consistent we shall present the basic results for $c=0.83$.

The angular distribution functions $f_1(t_2)$ and $f_2(t_2)$ in the c.m. frame for the $\alpha_1$ transitions from $2\,^1P_1$ and $2\,^3P_2$, respectively, at $E=102$ MeV/u are shown in Fig. 5. Both the components show a strong anisotropy, however, rotated by 90° to each other.

### E. $K\alpha_1$ transitions

Thus both $2\,^1P_1$ and $2\,^3P_2$ decays exhibit a rather large angular asymmetry. However, in the former case the distribution $f_1(t_2)$ reaches its largest values at $t_2=0$ (in the rest frame of the uranium ion), obtaining the minimum at $t_2^2=1$. In the latter case we face the opposite situation with the smallest value of the distribution reached at $t_2=0$. Now let us consider the observable superposition of these transitions.

The sum of the distributions (72) and (86) provides

$$\frac{d\sigma}{dt_2}=\frac{\alpha\omega_1}{8}T(p)^2\mathcal{F}(t_2) \tag{93}$$

with

$$\mathcal{F}(t_2)=\frac{4}{3}+5c+\frac{\lambda^2}{3}(4+5c)-t_2^2\frac{\lambda^2-1}{3}(4-5c). \tag{94}$$

The distribution $\frac{d\sigma}{dt_2}$ is symmetric with respect to $t_2=0$ ($\theta_{\mathrm{CM}}=\pi/2$). The anisotropy can be described by the parameter

$$\mu=\frac{\mathcal{F}(0)}{\mathcal{F}(1)}=\frac{4(1+\lambda^2)+5c(3+\lambda^2)}{8+10c(1+\lambda^2)}. \tag{95}$$

At $\lambda^2=3.92$, $c=0.83$ we find

$$\mu=0.99, \tag{96}$$

while $\mu=1.03$ for $c=0.70$. The function $f(t_2)$ defined by Eq. (4) is

$$f(t_2)=1.01-0.03t_2^2, \tag{97}$$

with an appreciable smaller anisotropy than in the transitions $2\,^1P_1$ and $2\,^3P_2$ to $1\,^1S_0$ considered separately. The angular distribution of the $K\alpha_1$ line for $E=102$ MeV/u in the laboratory frame is also shown in Fig. 5. Moreover, the angular distributions for both $K\alpha_{1,2}$ lines are depicted in Fig. 6, see below.

Note also that putting $c=1$ (see discussion at the end of the previous section) we find $\mu=0.95$, also corresponding to a pretty small anisotropy. Note further that the value of $\mu$ exhibits a very weak dependence on $\lambda^2$ and thus on the electron energy (in the limits of applicability of the nonrelativistic treatment of the incoming electron).

As we emphasized above, the $K\alpha_1$ line is a composition of $E1$ and $M2$ transitions. However, in this particular $M2$ transition the cancellation of the terms $t_2^4$ takes place at any value of the energy of the incoming electron. Thus the total function $f(t_2)$ can be presented by Eq. (5).

### F. $K\alpha_2$ transitions

The $K\alpha_2$ line is due to the transitions via the two-particle states formed by $1s_{1/2}$, $2s_{1/2}$ and $1s_{1/2}$, $2p_{1/2}$ electrons. In the former case the intermediate state is $2\,^3S_1$, decaying to the ground state by $M1$ transition. In the latter case the intermediate state is $2\,^3P_1$, with an $E1$ decay to the ground state.

In the case of the $2\,^3S_1$ intermediate state all the dependence of the coefficients $D_{1M}$ defined by Eq. (77) is contained in the spin functions $\kappa^2(1,M)$ introduced in Sec. IV A. Due to the normalization condition $\kappa^2(1,M)=1$, the terms $D_{1M}$ do not depend on $M$. Thus the contribution of the $2\,^3S_1$ state to the $K\alpha_2$ line is isotropic.

The case of the $2\,^3P_1$ state can be considered in the way similar to the treatment of the $K\alpha_1$ transition in the previous sections. We find

$$B_{10}^2=\frac{1-t_1^2}{3}\lambda^2T(p)^2;\quad B_{1,\pm1}^2=\frac{1+t_1^2}{6}T(p)^2$$

for the coefficients $B_{1M}$ which enter the rhs of Eq. (68). Thus the parameters $D_{1M}$ do depend on $M$ in this case, leading to a nonvanishing anisotropy.

Recall that the intermediate state $2\,^3P_2$ can decay to the ground state via the intermediate state $2\,^3S_1$. In the experiments such events are counted as contributions to the $K\alpha_2$ line. This transition can be shown to be isotropic (see Appendix B).

Superposition of these three contributions provides the angular distribution of the $K\alpha_2$ line

$$\frac{d\sigma}{dt_2}=\frac{\alpha\omega_1}{8}T(p)^2\left[16\left(1+\frac{p^2}{\eta_1^2}\right)+\frac{2}{3}[1+\lambda^2-t_2^2(\lambda^2-1)]+\frac{80}{9}(1-c)(\lambda^2+2)\right], \tag{98}$$

with $\eta_1=m\alpha Z$, $T(p)$ is obtained in Appendix A. The first and second terms in the external brackets on the rhs of Eq. (98) correspond to intermediate states $2\,^3S_1$ and $2\,^3P_1$, while the third one describes the decay of the $2\,^3P_2$ state via the $2\,^3S_1$ state.

Using Eq. (98) we find

$$\mu=1+\frac{\Lambda}{2}\frac{1}{1+12(1+p^2/\eta_1^2)+\frac{20}{3}(1-c)(\Lambda+3)}. \tag{99}$$

At $\varepsilon=50$ keV we obtain $\mu=1.05$. The deviation in the angular distributions from an isotropic one is shown in Fig. 6 for both the $K\alpha_{1,2}$ lines for $E=102$ MeV/u; for convenience laboratory angles are given. For the $K\alpha_2$ emission additionally the experimental data for the corresponding normalized anisotropy are shown. As these data refer to absolute line intensities huge systematic errors (of at least 10%) apply to the individual data points on top of the small statistical uncertainties. Within these large systematic errors a reasonable agreement can be stated. We emphasize that for line intensity ratios these systematic errors cancel and only statistical uncertainties have to be considered. The energy dependence of the anisotropy parameters both the for $K\alpha_{1,2}$ lines is presented in Fig. 7. The negligible positive anisotropy of the $K\alpha_1$ emission stays constant over the whole range; whereas the small negative anisotropy for the $K\alpha_2$ emission gets even smaller with increasing ion energy. For comparison, the large

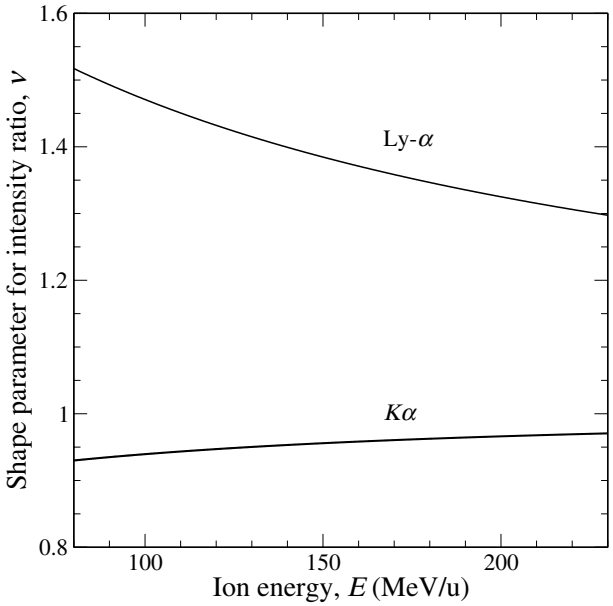


FIG. 9. The energy dependence for the shape parameter $\nu$ defined by the $K\alpha_1/K\alpha_2$ intensity ratio normalized to the emission at 0° see Eq. (101). For comparison the corresponding ratio Ly-$\alpha_1$/Ly-$\alpha_2$ is also represented.

anisotropy for the Ly-$\alpha_1$ emission for the initially bare ion case is shown too.

### G. Observable $K\alpha_1/K\alpha_2$ intensity ratio

Now we can calculate the $K\alpha_1/K\alpha_2$ intensity ratio which is observed in the experiment. Combining Eqs. (93), (94), and (98) we find

$$R(t_2) = \frac{2\left[\Lambda + 2 + 5c\left(1 + \frac{\Lambda}{4}\right) - t_2^2\Lambda\left(1 - \frac{5c}{4}\right)\right]}{24\left(1 + \frac{p^2}{\eta_1^2}\right) + \Lambda + 2 + \frac{40}{3}(1-c)(\Lambda+3) - \Lambda t_2^2}. \tag{100}$$

Using Eq. (12) we can obtain also the laboratory system ratio $R(t_2(\tau_2))$. The ratio of Eq. (100) for $E=102$MeV/u in the laboratory frame is shown in Fig. 8. One can see that our calculations are in good agreement with the experimental data. Our averaged value $R=0.45$ is also very close to the experimental value $R=0.43$.

Note that while the anisotropy is not sensitive to the actual value of $c$, the absolute values of the function $R(t_2)$ are. This is mainly due to the terms proportional to $1-c$ in the denominator of Eq. (100), corresponding to the effective $K\alpha_2$ line. For $c=0.70$ we would find the averaged value $R=0.54$.

To trace the energy dependence of the shape of the ratio $R(t_2)$ we normalize this ratio to the values at 90° and 0° (c.m. angles)

$$\nu = \frac{R(0)}{R(1)}. \tag{101}$$

The energy dependence of the parameter $\nu$ is presented in Fig. 9. As expected, the almost negligible anisotropy of the $K\alpha_1/K\alpha_12$ ratio gets even smaller with increasing energy. Comparing the theoretical results for the angular distributions $\alpha_1/\alpha_2$ for initially bare and H-like ions—see also Figs. 3(a) and 3(b)—we see that the anisotropy becomes almost negligible in the latter case. Since we neglected the interactions between the electrons, the strong change is due to the Pauli principle.

## V. SUMMARY

Radiative electron capture of quasifree target electrons into highly charged, very heavy ions can populate excited projectile states cascading down to the ground state by x-ray emission. The L-REC-cascade decay was studied at the heavy ion storage ring ESR for initially bare and hydrogenlike U ions typically around 100MeV/u. For intermediate $2p_{3/2}$ electrons the cascade radiation to the ground state (the Ly-$\alpha_1$ and $K\alpha_1$ radiation, respectively) experimentally shows emission patterns at strong variance: For initially bare ions a pronounced anisotropy of the Ly-$\alpha_1$ line was found, whereas for the case of initially hydrogenlike ions the $K\alpha_1$ line displays almost isotropy. In both cases the Ly-$\alpha_2$ and $K\alpha_2$ emission displays an isotropic emission within the experimental accuracies.

For both initially bare and initially H-like ions, the intermediate levels involving the captured $2p_{3/2}$ electron are strongly aligned. The alignment of the $2p_{3/2}$ electron is determined by the capture process avoiding an angular momentum transfer towards the collision direction and preferring an angular momentum in the intermediate state perpendicular to the ion direction. In the case of the initially bare ion this leads to the large negative $\beta_2$ values deduced from the strong Ly-$\alpha_1$ anisotropy and visa versa [cf. Figs. 3(a) and 4]. In the case of initially H-like ions, the captured and strongly aligned $2p_{3/2}$ electron will couple with the available $1s_{1/2}$ electron which itself shows no initial directional preference. The $m$ substate population of the $2p_{3/2}$ electron will be redistributed according to the coupling rules to the $m$ substates of the relevant two-electron states. Consequently, the $^1P_1$ and the $^3P_2$ states are corresponding to the $2p_{3/2}$ state strongly aligned. This leads in the end to the large anisotropy in the corresponding individual ground state transitions contributing to the $K\alpha_1$ emission (cf. Fig. 5). However, one transition is $E1$ and the other one $M2$, respectively; and as the $E$ and $H$ fields are perpendicular the equivalent alignment in both the states yields to emission patterns perpendicular to each other with the consequence of a cancellation of the anisotropy for the total $K\alpha_1$ emission (see Fig. 8). As was pointed out already in Refs. [17,29], it is interesting to note that in the case of the Ly-$\alpha_1$ emission the small $M2$ contribution which has to be added coherently to the $E1$ transition amplitudes enhances the anisotropy, whereas the incoherent addition of the $E1$ and $M2$ components yields to an almost isotropic emission of the total $K\alpha_1$ emission.

In order to elucidate this phenomenon, we carried out analytical calculations for the angular distribution both of Ly-$\alpha_1$ photons in radiative electron capture to the $L$ shell by the bare nucleus $U^{92+}$ and of $K\alpha_1$ photons in capture by the single-electron ion $U^{91+}$ (with a bound electron in the $1s$ state). We used the presentation of relativistic Coulomb functions as fast converging series in the parameter $(\alpha Z)^2$. We included only the lowest terms of the expansion, and took into account pure $E1$ type emission for the first photon.

We show that in the case of capture by a bare nucleus the intermediate state $2p_{1/2}$ (and $2s_{1/2}$) provides an isotropic angular distribution for the Ly-$\alpha_2$ photons, where for the intermediate state $2p_{3/2}$ the differential Ly-$\alpha_1$ emission cross section $\frac{d\sigma}{dt_2}$ at $t_2^2=0$ (i.e., $\theta_{\text{c.m.}}=\frac{\pi}{2}$) is at 90 MeV/u about 1.5 times larger than at $t_2^2=1$ (i.e., $\theta_{\text{c.m.}}=0$); including the weak $M2$ decay, this factor increases to about 1.7. This agrees reasonably well with the experimental data [1,12] and with the result of the calculations carried out in the framework of other approaches [14,17].

We show that in the case of capture by a hydrogenlike ion the angular distribution for the total $K\alpha_1$ emission $\frac{d\sigma}{dt_2}$ varies by less than 3% in the whole interval $0<t_2^2<1$. The effect is caused by the Pauli principle with the electron interactions being of minor importance. The results agree reasonably well with the experimental data. Moreover, we traced the energy dependence of the angular distributions and of the anisotropy parameters. The general tendency is that the anisotropy effects fade away with increasing energy. We like to point to quite recent numerical calculations applying a density matrix approach and using multiconfiguration Dirac-Fock wave functions yielding closely comparable results [30].

Our results are stable with respect to uncertainties of the experimental parameters and to the approximations made in the calculations. Going beyond these approximations would alter the theoretical results by about 10%. Moreover, cascades from capture to higher shells $(M,N,\ldots)$, which have not been treated in our approach, may also contribute to a minor modification of the emission characteristics. We emphasize, however, that in contrast to the total $K\alpha_1$ emission the separated ground state transitions from the intermediate $2\,^1P_1$ and $2\,^3P_2$ states show both an appreciable anisotropy but rotated by 90° to each other and, hence, compensate to near isotropy in the total emission.

Now we can discuss the role of various interactions involved in the process. The single-particle wave functions are determined by the central field strength. The interelectron interactions play the crucial role in the structure of the two-particle levels. For example, the splitting of $2\,^3P_2$ and $2\,^1P_1$ levels formed by $2p_{3/2}$ and $1s_{1/2}$ electrons is due to electron interactions. However, the magnitude of the anisotropy effects is determined mainly by the Pauli principle.

After integration of the angular distribution we find that the total cross section of two-photon capture to the ground state via a certain intermediate state $x$ is equal just to the cross section of the single-photon capture to the state $x$. This is because the sum of probabilities of the further decay of the state $x$ to the ground state over all possible channels is equal to unity.

In the present paper we carried out calculations in the lowest order of all the parameters which can be treated perturbatively. This enabled us to clarify the main mechanism of the difference of anisotropy effects in the cases of the hydrogenlike and heliumlike ions. The Pauli principle appeared to play the major role. The strong anisotropy of Ly-$\alpha_1$ emission in the hydrogenlike case contrasted to the negligible anisotropy of about 3% in the $K\alpha_1$ line in the heliumlike case. We obtained our results in analytical form, which enables us to trace the energy dependence of the characteristics of the processes investigated in the paper.

The powerful computer methods employed nowadays enable one to obtain more precise results by inclusion of higher order corrections and the subtle QED effects (see, e.g., [29]). This becomes increasingly important since the anisotropy effects in $K\alpha$ lines are small. However, the main mechanism is clarified in the present paper. The analytical and accurate numerical approaches to the problem would be complimentary to each other.

## ACKNOWLEDGMENTS

We thank L.N. Labzowsky for discussions and G. Palffy for assistance. Three of us (E.G.D., A.I.M., and I.A.M.) acknowledge hospitality during the visit to GSI and thank W. Scheid for hospitality during a stay at Justus-Liebig University at Giessen. This work was supported by the DFG grant 436 RUS 113/822/0-1.

## APPENDIX A

We start with calculation of the matrix element $B_{jm}$ presented by Eq. (33). Following Sec. III A it can be presented in the form

$$B_{jm}=(4\pi\alpha)^{1/2}\int\frac{d^3f}{(2\pi)^3}\psi_{jm}^*(\boldsymbol{f})\times\left(\frac{(\boldsymbol{e}\cdot\boldsymbol{f})}{m}+\frac{i}{2}\frac{(\boldsymbol{e}[\boldsymbol{\sigma}\boldsymbol{k}_1])}{m}\right)\psi_i(\boldsymbol{f}+\boldsymbol{k}_1),\tag{A1}$$

where the relativistic functions $\psi_{jm}$ and $\psi_i$ can be presented as $(\alpha Z)^2$ series. The integral (A1) is saturated by $f\sim p$. The spin-dependent term of the electron-photon interaction (the second term in the brackets of the integrand) provides the contribution to the values $B_{jm}^2$ which is $(\omega_1/p)^4\sim 10^{-2}$ times smaller than that of the first term and thus can be neglected. Hence we put

$$B_{jm}=(4\pi\alpha)^{1/2}\int\frac{d^3f}{(2\pi)^3}\psi_{jm}^*(\boldsymbol{f})\frac{(\boldsymbol{e}\cdot\boldsymbol{f})}{m}\psi_i(\boldsymbol{f}+\boldsymbol{k}_1),\tag{A2}$$

which we calculate by using the nonrelativistic functions, i.e., the lowest order terms of $(\alpha Z)^2$ series. As we have seen in Sec. III C the higher order terms provide the corrections of the order 10% in our case.

We employ the presentation of the Coulomb functions in the form suggested in [26]

$$\psi_{jm}(\boldsymbol{f})=\left(\frac{4\pi}{3}\right)^{1/2}N_2\eta_2(\boldsymbol{\Omega}_{jm}\cdot\boldsymbol{\nabla}_q)\left(-\frac{\partial}{\partial\eta_2}\right)\langle\boldsymbol{f}|V_{i\eta_2}|\boldsymbol{q}\rangle\tag{A3}$$

with $\boldsymbol{q}=\boldsymbol{0}$, while $\eta_2=\frac{m\alpha Z}{2}$, $N_2=(\eta_2^3/\pi)^{1/2}$, and

$$\langle \boldsymbol{f}|V_{i\eta}|\boldsymbol{q}\rangle = \frac{4\pi}{(\boldsymbol{f}-\boldsymbol{q})^2+\eta^2} \tag{A4}$$

for any vectors $\boldsymbol{f}$ and $\boldsymbol{q}$.

The continuum wave function with asymptotic momentum $\boldsymbol{p}$ is [19]

$$\psi_i(\boldsymbol{f}) = N(\xi)\left(-\frac{\partial}{\partial\nu}\right)J_x\langle \boldsymbol{p}(1-x)|V_{px+i\nu}|\boldsymbol{f}\rangle \tag{A5}$$

with $N(\xi)=\left[\frac{2\pi\xi}{1-\exp(-2\pi\xi)}\right]^{1/2}$, $\xi=\frac{m\alpha Z}{p}$, $\nu=0$, and

$$J_x = \frac{1}{2\pi i}\oint \frac{dx}{x}\left(\frac{-x}{1-x}\right)^{i\xi}.$$

Presenting

$$\left(-\frac{\partial}{\partial\eta_2}\right)\boldsymbol{f}\langle \boldsymbol{f}|V_{i\eta_2}|\boldsymbol{k}\rangle = \left(\eta_2\boldsymbol{\nabla}_k - \boldsymbol{k}\frac{\partial}{\partial\eta_2}\right)\langle \boldsymbol{f}|V_{i\eta_2}|\boldsymbol{q}\rangle,$$

and carrying out the integration over $\boldsymbol{f}$ by using

$$\int \frac{d^3f}{(2\pi)^3}|\boldsymbol{f}\rangle\langle\boldsymbol{f}| = 1; \quad \left(-\frac{\partial}{\partial\eta}\right)V_{i\eta}V_{i\tau} = V_{i\eta+i\tau},$$

we obtain

$$B_{jm} = \frac{(4\pi\alpha)^{1/2}}{m}\left(\frac{4\pi}{3}\right)^{1/2}N(\xi)N_2a_2 \times[\eta_2(\boldsymbol{\Omega}^*_{jm}\cdot\boldsymbol{\nabla}_k)(\boldsymbol{e}_1\cdot\boldsymbol{\nabla}_k) - (\boldsymbol{\Omega}^*_{jm}\cdot\boldsymbol{e}_1)]U(\boldsymbol{p},\boldsymbol{k}) \tag{A6}$$

with

$$U(\boldsymbol{p},\boldsymbol{k}) = \frac{4\pi}{(\boldsymbol{p}-\boldsymbol{k})^2+\eta_2^2}\left[\frac{(\boldsymbol{p}-\boldsymbol{k})^2+\eta_2^2}{k^2-(p+i\eta_2)^2}\right]^{i\xi} \tag{A7}$$

and $\boldsymbol{k}=\boldsymbol{k}_1$.

After the calculation of the derivatives on the rhs of Eq. (A6) we must put $\boldsymbol{k}=0$. The amplitude $B_{jm}$ is thus expressed in the terms of the function

$$V(p) = \frac{1}{a(p)}\left(\frac{a(p)}{b(p)}\right)^{i\xi} \tag{A8}$$

with

$$a(p) = p^2+\eta_2^2, \quad b(p) = -(p+i\eta_2)^2. \tag{A9}$$

This leads to

$$B_{jm} = (4\pi\alpha)^{1/2}\left(\frac{4\pi}{3}\right)^{1/2} \times K\left[\frac{(\boldsymbol{\Omega}^*_{jm}\cdot\boldsymbol{e}_1)}{b(p)} + \frac{(\boldsymbol{\Omega}^*_{jm}\cdot\boldsymbol{p})(\boldsymbol{p}\cdot\boldsymbol{e}_1)}{a(p)^2}(i\xi-1)(i\xi-2)\right]V(p) \tag{A10}$$

with

$$K = \frac{4\pi}{m}N_2N(\xi)\eta_1^2. \tag{A11}$$

Thus the function $T(p)$ introduced in Sec. III B can be presented as

$$T(p) = K\frac{V(p)}{b(p)} \tag{A12}$$

with $K$, $V(p)$, and $b(p)$ defined by Eqs. (A11), (A8), and (A9).

Calculation of the function $T^s(p)$—Eq. (41)—can be done in a similar way. It is

$$T^s(p) = 8\pi\eta_1N_2N(\xi)(1-i\xi)\frac{pV(p)}{ma(p)}. \tag{A13}$$

## APPENDIX B

The dependence of the square of the amplitude $F^2$ on the angular variable $t_2$ of the last step photon in the three-photon transition from the continuum to $2\,^3P_2$ state with further $2\,^3P_2 \to 2\,^3S_1 \to 1\,^1S_0$ decay is determined by the function

$$y(t_2) = \sum_M A^2_{1M}(t_2)a_M \tag{B1}$$

with

$$a_M = \sum_{M'}\int dt_i dt_1 X^2_{1M,2M'}(t_i)B^2_{2M'}(t_1). \tag{B2}$$

Here $B_{2M'}$, $X_{1M,2M'}$, and $A_{1M}$ are the amplitudes of the emission of the first photon in REC to the $2\,^3P_2$ state, of radiation of "intermediate" photon in the transition of the state $2\,^3P_2$ to $2\,^3S_1$, and of the "second" photon of the transition $2\,^3S_1 \to 1\,^1S_0$. The corresponding angular variables are $t_1$, $t_i$, and $t_2$, $M$ and $M'$ are the projections of the angular momenta. Summation over the polarizations of the photons is carried out.

Note that

$$\int dt_i X^2_{1M,2M'}(t_i) = x \tag{B3}$$

does not depend on $M$ and $M'$. Hence

$$a_M = x\sum_{M'}\int dt_1 B^2_{2M'}(t_1) \tag{B4}$$

does not depend on $M$. Thus

$$y(t_2) = a\sum_M A^2_{1M}(t_2) \tag{B5}$$

does, indeed, not depend on $t_2$, since the sum on the rhs of Eq. (B5) does not depend on $t_2$. Thus this transition is isotropic.

[1] Th. Stöhlker *et al.*, Phys. Rev. Lett. **79**, 3270 (1997).
[2] X. Ma *et al.*, Phys. Rev. A **68**, 042712 (2003).
[3] J. Eichler and W. E. Meyerhof, *Relativistic Atomic Collisions* (Academic Press, San Diego, 1995).
[4] Th. Stöhlker *et al.*, Phys. Rev. A **51**, 2098 (1995).
[5] Th. Stöhlker, C. Kozhuharov, P. H. Mokler, and A. Warczak, Comments At. Mol. Phys. **33**, 271 (1997).
[6] Th. Stöhlker *et al.*, Phys. Scr., T **73**, 252 (1997).
[7] Th. Stöhlker *et al.*, Phys. Lett. A **238**, 43 (1998).
[8] Th. Stöhlker *et al.*, Phys. Rev. Lett. **82**, 3232 (1999).
[9] Th. Stöhlker *et al.*, Phys. Scr., T **80**, 379 (1999).
[10] Th. Stöhlker *et al.*, Phys. Rev. Lett. **86**, 983 (2001).
[11] X. Ma *et al.*, Nucl. Phys. Rev. **19**, 2 (2002).
[12] G. Bednarz *et al.*, Hyperfine Interact. **146/147**, 29 (2003).
[13] G. Bednarz *et al.*, Nucl. Instrum. Methods Phys. Res. B **235**, 280 (2005).
[14] Th. Stöhlker *et al.*, Phys. Scr., T **110**, 384 (2004).
[15] A. Ichihara, T. Shirai, and J. Eichler, Phys. Rev. A **54**, 4954 (1996).
[16] P. H. Mokler and Th. Stöhlker, Adv. At., Mol., Opt. Phys. **37**, 297 (1996).
[17] A. Surzhykov, S. Fritzsche, A. Gumberidze, and Th. Stöhlker, Phys. Rev. Lett. **88**, 153001 (2002).
[18] E. Spindler, H.-D. Betz, and F. Bell, Phys. Rev. Lett. **42**, 832 (1979).
[19] V. G. Gorshkov, Zh. Eksp. Teor. Fiz. **40**, 1481 (1961).
[20] C. G. Darwin, Proc. R. Soc. London, Ser. A **118**, 654 (1928).
[21] W. H. Furry, Phys. Rev. **46**, 391 (1934).
[22] A. Sommerfeld and A. W. Maue, Ann. Phys. **22**, 629 (1935).
[23] J. Eichler, Phys. Rep. **193**, 165 (1990).
[24] V. G. Gorshkov and A. I. Mikhailov, Zh. Eksp. Teor. Fiz. **43**, 991 (1962).
[25] L. F. Vitushkin and A. I. Mikhailov, Zh. Eksp. Teor. Fiz. **70**, 1762 (1976) [Sov. Phys. JETP **43**, 917 (1976)].
[26] V. G. Gorshkov, A. I. Mikhailov, and S. G. Sherman, Zh. Eksp. Teor. Fiz. **66**, 2020 (1974) [Sov. Phys. JETP **39**, 995 (1974)].
[27] J. Eichler, A. Ichihara, and T. Shirai, Phys. Rev. A **58**, 2128 (1998).
[28] F. A. Parpia, C. Froese Fisher, and I. P. Grant, Comput. Phys. Commun. **94**, 249 (1996).
[29] A. N. Artemyev, V. M. Shabaev, V. A. Yerokhin, G. Plunien, and G. Soff, Phys. Rev. A **71**, 062104 (2005).
[30] A. Surzhykov (private communication); A. Surzhykov, U. D. Jentschura, Th. Stöhlker, and S. Fritzsche (unpublished).